

DETERMINATION OF STRESSES IN VLASOV BEAM SECTIONS

A THESIS SUBMITTED TO
THE GRADUATE SCHOOL OF NATURAL AND APPLIED SCIENCES
OF
MIDDLE EAST TECHNICAL UNIVERSITY

BY

SEMIH ERDOĞAN

IN PARTIAL FULFILLMENT OF THE REQUIREMENTS
FOR
THE DEGREE OF MASTER OF SCIENCE
IN
MECHANICAL ENGINEERING

SEPTEMBER 2019

Approval of the thesis:

DETERMINATION OF STRESSES IN VLASOV BEAM SECTIONS

submitted by **SEMIH ERDOĞAN** in partial fulfillment of the requirements for the degree of **Master of Science in Mechanical Engineering Department, Middle East Technical University** by,

Prof. Dr. Halil Kalıpçılar
Dean, Graduate School of **Natural and Applied Sciences**

Prof. Dr. M.A. Sahir Arıkan
Head of Department, **Mechanical Engineering**

Prof. Dr. Suha Oral
Supervisor, **Mechanical Engineering, METU**

Examining Committee Members:

Prof. Dr. Haluk Darendeliler
Mechanical Engineering, METU

Prof. Dr. Suha Oral
Mechanical Engineering, METU

Prof. Dr. Serkan Dağ
Mechanical Engineering, METU

Prof. Dr. Can Çoğun
Mechatronics Engineering, Çankaya University

Assoc. Prof. Dr. Uğur Polat
Civil Engineering, METU

Date: 06.09.2019

I hereby declare that all information in this document has been obtained and presented in accordance with academic rules and ethical conduct. I also declare that, as required by these rules and conduct, I have fully cited and referenced all material and results that are not original to this work.

Name, Surname: Semih Erdoğan

Signature:

ABSTRACT

DETERMINATION OF STRESSES IN VLASOV BEAM SECTIONS

Erdoğan, Semih
Master of Science, Mechanical Engineering
Supervisor: Prof. Dr. Suha Oral

September 2019, 68 pages

In this thesis, the normal and shear stresses in Vlasov beams are determined. The shape of the considered cross-sections may be arbitrary. For the computation of shear stresses, two-dimensional triangular finite element formulations are developed. The stiffness matrices and force vectors are derived for transversal forces, uniform torsion, and nonuniform torsion. The proposed finite element algorithm is validated through the analytical solutions, structural engineering books, and related articles. The numerical examples include beams with different cross-section types such as solid, thick-walled, closed thin-walled, and open thin-walled sections.

Keywords: Vlasov Beams, Finite Element Method, Normal and Shear Stresses, Cross-section properties, Warping Function

ÖZ

VLASOV KİRİŞ KESİTLERİNDE GERİLİMLERİN BELİRLENMESİ

Erdoğan, Semih
Yüksek Lisans, Makina Mühendisliği
Tez Danışmanı: Prof. Dr. Suha Oral

Eylül 2019, 68 sayfa

Bu tezde, Vlasov kirişlerinde normal ve kayma gerilmeleri belirlenir. Ele alınan kesitlerin şekli isteğe bağlı olabilir. Kayma gerilmelerinin hesaplanması için iki boyutlu üçgensel sonlu elemanlar formülasyonları geliştirilir. Kayma yüklemeleri, düzenli burulma ve düzensiz burulmalar için sertlik matrisleri ve yük vektörleri türetilir. Önerilen sonlu elemanlar algoritması analitik çözümler, yapısal mühendislik kitapları ve ilgili makalelerle doğrulanır. Sayısal örnekler, dolu kesitli, kalın duvar kesitli, kapalı ve açık ince duvarlı kesitli gibi farklı enine kesit tiplerine sahip kirişler içerir.

Anahtar Kelimeler: Vlasov Kirişleri, Sonlu Elemanlar Yöntemi, Normal ve Kayma Gerilmeleri, Kesit Alanı Özellikleri, Çarpılma Fonksiyonu

To my deceased father Hüsamettin Erdoğan and my family

ACKNOWLEDGEMENTS

I would like to express my gratitude to my supervisor Prof. Dr. Suha Oral, for giving me an opportunity to work with him, allowing me to benefit from his invaluable comments and experiences and his endless patience throughout my study.

TABLE OF CONTENTS

ABSTRACT	v
ÖZ.....	viii
ACKNOWLEDGEMENTS	viii
TABLE OF CONTENTS	ix
LIST OF TABLES	xi
LIST OF FIGURES	xii
LIST OF ABBREVIATIONS	xiv
LIST OF SYMBOLS	xv
CHAPTERS	
1. INTRODUCTION	1
1.1. Introduction	1
1.2. Thesis Objective	3
1.3. Thesis Plan	3
2. LITERATURE REVIEW.....	5
2.1. Analytical Solutions	5
2.2. Numerical Solutions	6
3. FORMULATIONS	9
3.1. Governing Equations and Internal Forces in Beams	9
3.2. Determination of Stresses	18
3.2.1. Stresses due to Normal Force and Bending Moments	19
3.2.2. Stresses due to Shear Forces	19
3.2.3. Stresses due to Saint Venant's Torque	22

3.2.4. Stresses due to Warping Moment and Warping Torque	27
4. NUMERICAL EXAMPLES	31
4.1. Solid Sections	31
4.1.1. Rail Section.....	31
4.1.2. Elliptical Section.....	34
4.1.3. Variable Section.....	37
4.2. Thick-walled Sections	45
4.2.1. Hollow Square Section.....	45
4.3. Thin-walled Open Sections	48
4.3.1. Channel Section	48
4.4. Thin-walled Closed Sections.....	55
4.4.1. Multicell Section.....	55
5. CONCLUSIONS	61
5.1. Summary	61
5.2. Conclusion	61
5.3. Future Works.....	62
REFERENCES	63
APPENDICES	
A. DIN 536 Design Specification	67

LIST OF TABLES

TABLES

Table 4.1. Comparison of Cross-section Properties for the Rail Section	32
Table 4.2. Input Values for the Elliptical Section	35
Table 4.3. Comparison of the Shear Stresses over the Elliptical Section	35
Table 4.4. Comparison of the Warping Functions over the Elliptical Section.....	36
Table 4.5. Material Properties for the Beam of Variable Cross-section.....	38
Table 4.6. Comparison of Torsional Rigidities for the Beam	39
Table 4.7. Comparison of Warping Rigidities for the Beam	39
Table 4.8. Internal Forces for the Beam.....	40
Table 4.9. Comparison of the Warping Normal Stresses for the Channel Section ...	52
Table 4.10. Comparison of the St. Venant Shear Stresses for Channel Section	53
Table 4.11. Comparison of the Warping Shear Stresses for the Channel Section	54
Table 4.12. Material Properties for the Multicell Section.....	55
Table 4.13. Comparison of the Cross-section Properties for the Multicell Section ..	57
Table 4.14. Internal Forces for the Multicell Section	57
Table 4.15. Comparison of the Warping Functions for the Multicell Section	58
Table 4.16. Comparison of the Shear Stresses of the Multicell Section	59
Table 4.17. Comparison of the Normal Stresses of the Multicell Section.....	59

LIST OF FIGURES

FIGURES

Figure 1.1. Representation of Numerical Methods.....	1
Figure 1.2. Uniform Torsion and Non-uniform Torsion.....	2
Figure 3.1. 3-D Representation of a Beam with Arbitrary Cross-section.....	9
Figure 3.2. Representation of Triangular Element	12
Figure 3.3. yz and rs Coordinates Frame	14
Figure 3.4. Normal Vectors in Arbitrary Cross Section	16
Figure 3.5. Shear Center and Centroid in Arbitrary Cross Section	18
Figure 4.1. Loading Type and Meshed Geometry for the Rail Section.....	31
Figure 4.2. Comparison of Shear Flows for the Rail Section.....	32
Figure 4.3. Comparison of the Shear Stresses for the Rail Section (MPa)	33
Figure 4.4. Comparison of the Warping Functions for the Rail Section (mm ²)	33
Figure 4.5. Geometrical Parameters and Meshed Model for the Elliptical Section ..	34
Figure 4.6. Shear Stress Distribution over the Elliptical Section (MPa)	35
Figure 4.7. Variations of the Stresses in terms of the Number of Elements (MPa) ..	36
Figure 4.8. Comparison for the Warping Functions over the Elliptical Section (mm ²)	36
Figure 4.9. Geometrical Dimensions for the Beam of Variable Cross-section.....	37
Figure 4.10. Cross-sections located at Fixed End 1 (left), Middle, Fixed End 2 (right)	38
Figure 4.11. Discretization of the Beam	39
Figure 4.12. Variation of the Shear Stresses along the Beam at Point A	41
Figure 4.13. The Absolute Resultants of the Warping Shear Stresses (kPa)	42
Figure 4.14. The Absolute Resultants of the St. Venant Shear Stresses (kPa)	42
Figure 4.15. Variation of the Normal Stresses along the Beam at Point B.....	43
Figure 4.16. Distribution of the Normal Stresses (kPa).....	44

Figure 4.17. Hollow Square with Uniform Thickness	45
Figure 4.18. Distribution of the Torsional Constant in terms of Thickness/Length..	46
Figure 4.19. Discretization of the Hollow Square	46
Figure 4.20. Shear Stress Distributions for the Hollow Square (MPa).....	47
Figure 4.21. Channel Beam Problem under Torsional Moment	48
Figure 4.22. Distribution of the Angle of Twist	49
Figure 4.23. Distribution of the Saint Venant Torque	49
Figure 4.24. Distribution of the Warping Torque.....	50
Figure 4.25. Distribution of the Warping Moment.....	50
Figure 4.26. Stress Distribution for the Warping Moment at the fixed end (MPa)...	51
Figure 4.27. Stress Distribution for the St. Venant Torque at the free end (MPa)	52
Figure 4.28. Stress Distribution for the Warping Torque at fixed end (MPa)	53
Figure 4.29. Shear Flows under St. Venant and Warping Torque.....	54
Figure 4.30. 3D Representation of the Multicell Section under Applied Loadings ..	55
Figure 4.31. Thin-walled Representation of the Multicell Section	56
Figure 4.32. Numbering for the Thin-walled Solution	56
Figure 4.33. Distribution of the Warping Functions for the Multicell Section (MPa)	58
Figure 4.34. Distribution of the Shear Stresses of the Multicell Section (MPa)	58
Figure 4.35. Distribution of the Normal Stresses of the Multicell Section (MPa)	59

LIST OF ABBREVIATIONS

FE	Finite Element
FEM	Finite Element Method
FEA	Finite Element Analysis
BEM	Boundary Element Method

LIST OF SYMBOLS

u	Translational displacement in y-direction
v	Translational displacement in z-direction
θ	Rotational displacement in x-direction
y_o	Y coordinate of shear center w.r.t centroid
z_o	Z coordinate of shear center w.r.t centroid

CHAPTER 1

INTRODUCTION

1.1. Introduction

Beams are structural elements used in modeling various engineering structures such as aircraft wings, aircraft frames, helicopter rotor blades, automobile chassis, and edge beams in buildings. There are multiple different cross-section types of beams such as solid, thick-walled, thin-walled closed, and thin-walled open sections. The structural behavior of beams is characterized by the material they are made of and their geometry. Geometrical features play an important role in their behavior. The amount of deflection in a beam is directly related to its length while cross-sectional shape affects stresses occurring on the beam section. For this reason, the accuracy of cross-section properties is crucial for reliable stress analysis. While performing beam analyses under transversal and torsional loadings, it is necessary to obtain complicated section properties such as the shear center, torsional constant, and warping constant. For structures having a complex shape, it is difficult to calculate these properties by analytical means. To compute these parameters, numerical methods such as the boundary element method, the finite difference method, and the finite element method are needed.

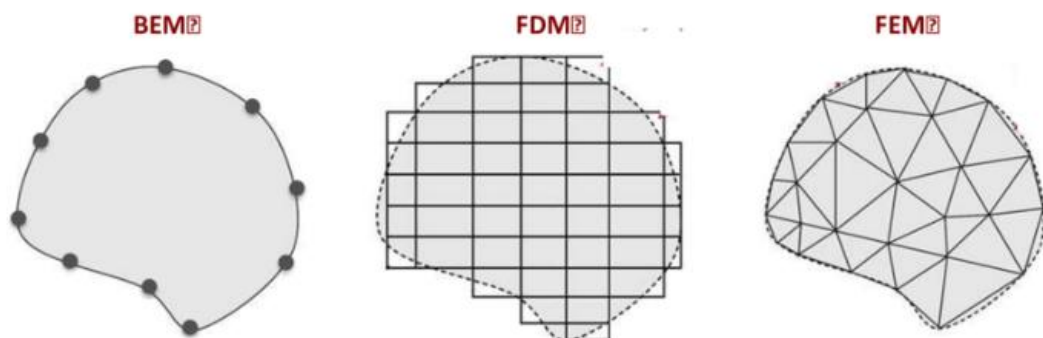


Figure 1.1: Representation of Numerical Methods [1]

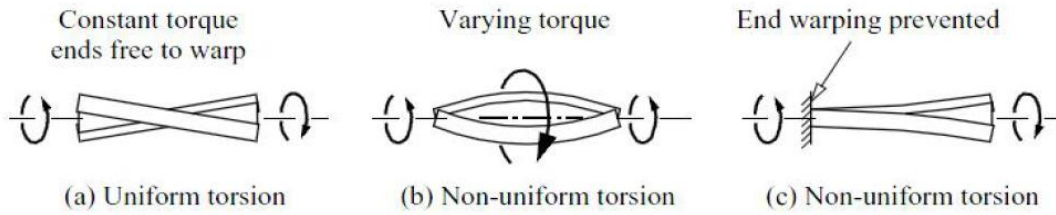


Figure 1.2: Uniform Torsion and Non-uniform Torsion [2]

In solid mechanics, it is crucial to comprehend the analysis of structures subjected to twisting moments correctly. For this reason, torsion has long been the subject of theoretical and practical interest in this field. The Saint Venant torsion theory [3] is referred to as uniform torsion and The Vlasov torsion theory [4] is known as nonuniform torsion. In the historical development of these works, Agustin Cauchy [5] demonstrated experimentally that non-circular beams under a torsional loading experience an out-of-plane displacement called warping. Based upon this, Saint Venant defined an axial displacement, which is a function of the in-plane direction. In uniform torsion, the warping displacement and angle of twist rate become identical in all cross-sections. This theory is valid if the beam is free to warp at the ends under constant torque. However, in more realistic cases, beams usually have boundary conditions. In other words, the warping and twist can be restrained at one or more cross-sections. Vlasov presented the nonuniform torsion theory. In this theory, the torque varies along the beam, or it is not free to warp at any cross-section. In a parallel manner to this, the angle of twist rate and axial displacement along its axis are not constant. These effects result in some internal forces such as warping moments and warping torques. In general, the warping effects are taken into account if the section type is open thin-walled since it has low torsional rigidities. For a conservative design, beam structures are analyzed considering not only the effect of Saint-Venant torsion but also the warping effects for all types of beams.

1.2. Thesis Objective

The purpose of this thesis is to determine cross-section properties and stresses in Vlasov beam sections using the finite element method. In the formulations of this study, the stiffness matrices and force vectors for transversal shear forces, uniform torsion, and non-uniform torsion are offered. For the discretization of the geometry, the numerical model uses 2D triangular mesh elements. This mesh type makes dealing with complex cross-sectional shapes possible. In the development of this study, several engineering software tools are integrated. As a pre-processor, Hypermesh provides input data with node coordinates and element connectivities of the meshed geometry. As a processor, Fortran organizes the FEM algorithm and solves the equilibrium matrix equations. As a post-processor, Tecplot visualizes output data with stress distributions, shear flow graphs, and warping characteristics. In numerical examples, beams with solid, thick-walled, open thin-walled, and closed thin-walled sections are used. Materials defined in the problems are homogeneous, isotropic, and linearly elastic. The reliability of the presented finite element algorithm is confirmed by already existing analytical solutions and the literature.

1.3. Thesis Plan

This dissertation is comprised of five chapters. It starts with Chapter 1 introducing the problem outline, thesis objective, and thesis plan. In Chapter 2, the related studies are represented in a literature review which focuses on previous works. This chapter also includes the analytical and numerical approaches to cross-sectional analyses. In Chapter 3, the formulations are separated into two subchapters. The first part deals with the internal forces on cross-sections. In the second part of Chapter 3, normal and shear stress equations are formulated. Chapter 4 verifies the proposed finite element model by comparing those found in the literature. Finally, Chapter 5 presents a conclusion as a result of the issues covered in the earlier chapters. This chapter also addresses recommendations for future researches in this area.

CHAPTER 2

LITERATURE REVIEW

This chapter is comprised of two subchapters that review analytical solutions and numerical solutions such as the boundary element method, the finite difference method, and the finite element method. In these subchapters, previous works in the literature related to the determination of cross-section properties and stresses on cross-sections are mentioned.

2.1. Analytical Solutions

E. Reissner and W. T. Tsai [6] proposed a mathematical solution to determine the centers of shear and twist for cylindrical shell beams by combining the Saint Venant torsion and flexure solutions with an appropriate version of the principle of minimum complementary energy. Similarly, E. Trefftz [7] and A. Weinstein [8] presented the analytical formulations of the centers of shear and twist for solid cross-section beams.

W. F. Chen, T. Atsuta [9] offered an analytical solution based on the Laplace equation for torsion analysis of structures having I-beam, C-beam, and T-Beam cross-sections by dividing them into rectangular sub-domains. In this study, the authors ignored corner fillets in the formulation.

Hematiyan and Doostfatemeleh [10] presented an approximate analytical method for a hollow isotropic polygonal shape under torsional loading. This method enabled the authors to estimate the variation of the shearing stress across the thickness of the beam. Although this method provided acceptable results for thin-walled and thick-walled beams, it did not address cover beams with open sections.

Timoshenko, J. Goodier [11] and J. J. Connor [12] explained uniform torsion theory called Saint Venant Theory in their textbooks in detail. Similarly, non-uniform torsion

theory in the presence of warping shear and normal stresses for thin-walled beams is addressed in the textbooks of V. Z. Vlasov [4] and Gjelsvik [13].

M. A. Gurel, R. K. Pekgokgoz, M. Kisa [14] proposed an approximated model and mathematical formulation for the uniform torsion analysis of thin-walled, thick-walled, and solid cross-sections. In their article, the formulas for the maximum shearing stress and the angle of twist was derived. They compared the results with several cross-sections having exact or numerical solutions. According to the obtained results, the formulations gave highly accurate values for thin-walled sections. For thick-walled and solid ones, however, this accuracy decreased gradually.

J. Francu, P. Novackova, P. Janicek [15] suggested an analytical solution for the constant cross-section using the Airy stress function. The contribution dealt with triangular, rectangular, and some other profiles. In the formulations, the authors solved the rectangular profile case through Fourier series.

2.2. Numerical Solutions

Katori, H. [16] implemented formulations to determine the shear center of arbitrary cross-sections using the finite element method. The author derived equations concerning the warping, angle of twist, shear deflection and Lagrange's multipliers. In the case study, the change of the coordinates of the shear center and centroid of the circular cross-sections by circular notches of various diameters were investigated. This problem was validated by the analytical solution of W.J. Strong, and T.G. Zhang [17].

B. D. Mixon [18] developed a finite element tool for the calculation of beam cross-section properties. In this thesis, warping independent and warping dependent cross-section properties were achieved using three-node triangles and six node triangles. The results were validated with Beam Tool of ANSYS which is a commercial software program that is highly useful in determining said properties.

G. H. Holze, C. P. Pulver, and Y. G. Giorgis [19] divided cross-section properties into basic and advanced ones such that the basic properties were area and centroids, and the advanced properties were torsional constants and the shear centers. They developed a boundary element method to solve the equations of Laplace and Poisson.

F. Gruttmann, R. Sauer, and W. Wagner [20] proposed approximate calculations of shear stresses in prismatic beams exposed to pure torsion and torsion-free bending using the finite element method. For numerical calculations, Dirichlet boundary conditions of torsion-free bending problems are converted into Neumann boundary conditions.

D. Banić, G. Turkalj, J. Brnić [21] developed a two-dimensional finite element formulation for the stress analysis of elastic beams with arbitrary cross-sections subjected to non-uniform torsion. The element stiffness matrix and load vectors were obtained by primary warping functions corresponding to uniform torsion and secondary warping functions to corresponding non-uniform torsion. The accuracy of the presented algorithm was validated with analytical solutions of I-Beams and C-Beams [9][22].

A. Stefan, M. Lupoae, D. Constantin, C. Baciú [23] aimed to determine the tangential stresses of rectangular sections and L-sections subjected to uniform torsion using the finite difference method. They concluded that the method displayed difficulties in some areas of use, such as when applied to curved boundary domains.

El Darwish and Johnston [24] applied an approximate method to perform torsion analyses of some structural shapes, such as T-beams, by using Prandtl's stress function via the finite difference method. They offered a formulation for the value of the torsional rigidity and shearing stress at the midpoint of the T-beam flanges. However, it is impossible to find shearing stress at the web-flange junction fillet by this method.

Lamancusa and Saravanos [25] presented the torsional analysis of hollow square tubes by a two-dimensional thermal analogy using the finite element method. They evaluated the dependence of torsional properties on wall thickness. The obtained

results were used to generate closed-form algebraic expressions for maximum shear stress and torsional stiffness.

Sapountzakis and Mokos [26] developed a boundary element method for bars with arbitrary cross-sections subjected to an arbitrarily distributed or concentrated twisting moment. The proposed procedure took into account the warping effects along the member length.

Walter Pilkey [27], in the book *Analysis and Design of Elastic Beams*, explained all forms of loading conditions that can be subjected to beams. Based on these explanations, two programs named *ThinWall* and *PlotStress* were developed; these programs took advantage of the finite element method.

CHAPTER 3

FORMULATIONS

3.1. Governing Equations and Internal Forces in Beams

In Figure 3.1, a beam with arbitrary cross section is shown in three-dimensional view. In this thesis, all derivations and solutions are evaluated according to the coordinate system shown in Figure 3.1.

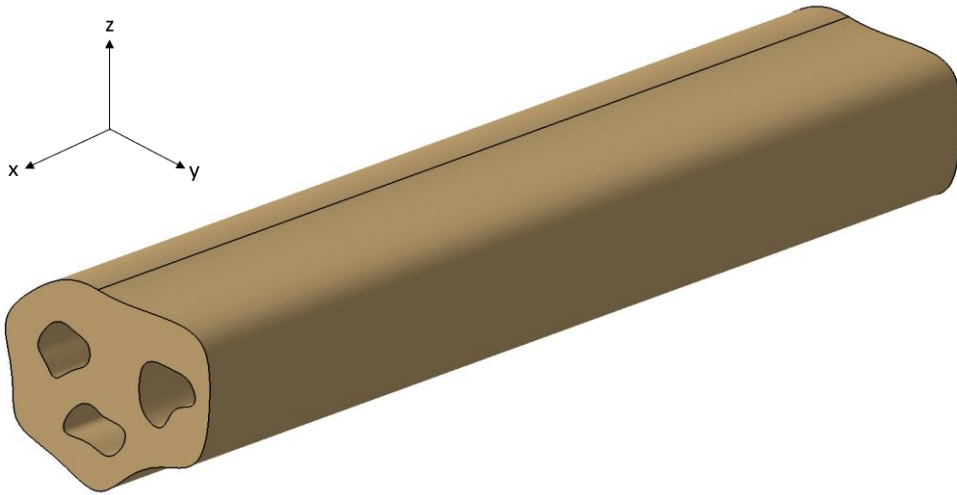


Figure 3.1: 3-D Representation of a Beam with Arbitrary Cross-section

The governing equations of a beam are

$$EA(u'' - \alpha\Delta T') = -f_x$$

$$E(I_y I_z - I_{yz}^2)v^{iv} = I_y f_y + I_{yz} f_z$$

$$E(I_y I_z - I_{yz}^2)w^{iv} = I_z f_z + I_{yz} f_y$$

$$EI_w \theta^{iv} - GJ\theta'' = m_x$$

(3.1)

where θ is the angle of twist, u , v , w and f_x , f_y , f_z are the displacements and the intensities of distributed forces in x , y , z directions, respectively, m_x is the intensity of distributed torque, ΔT is the thermal force, E is the elasticity modulus, G is the shear modulus, α is thermal expansion coefficient of the beam material, A is the area, I_y , I_z , I_{yz} are the second moments of area, J is the torsional constant and I_w is the warping constant of the cross section.

Then, the stress resultants in a cross section are

$$\begin{aligned}
N &= EA(u' - \alpha\Delta T) \\
M_y &= EI_{yz}v'' - EI_yw'' \\
M_z &= EI_zv'' - EI_{yz}w'' \\
M_w &= EI_w\theta'' \\
S_y &= EI_{yz}w''' - EI_zv''' \\
S_z &= EI_{yz}v''' - EI_yw''' \\
M_x &= GJ\theta' - EI_w\theta''' \\
T_s &= GJ\theta' \\
T_w &= -EI_w\theta''' \\
T &= T_s + T_w
\end{aligned} \tag{3.2}$$

where N is the axial force, S_y , S_z are the shear forces, M_y , M_z are the bending moments, M_w is the warping moment, T_s is the St.Venant torque, T_w is the warping torque, and T is the total torque acting on the cross section. The resultants are calculated either by solving the governing equations or by using a computational method. One of the choices in computational methods is the finite element analysis. The resultants N , M_y , M_z , S_y , S_z are obtained by using the standard bar and Euler-Bernoulli beam finite elements. The resultants T_s , T_w , M_w can be obtained by a torsion finite element.

Torsion Finite Element

The weak form of the torsion equation is

$$\int g(EI_w \theta'' - GJ\theta'' - m_x) dx = 0$$

where $g(x)$ is a test function. Using integration by parts, the weak form can be expressed as

$$EI_w \int g'' \theta'' dx + GJ \int g' \theta' dx = (gT)_B + (g'M_w)_B + \int g m_x dx$$

where the subscript B indicates the boundaries. Consider a finite element of length L with node-1 at $x = 0$ and node-2 at $x = L$.

The twist angle θ can be assumed as

$$\theta = \mathbf{\Omega} \boldsymbol{\delta}$$

where

$$\mathbf{\Omega} = \frac{1}{L^3} [(L + 2x)(L - x)^2 \quad Lx(L - x)^2 \quad x^2(3L - 2x) \quad Lx^2(x - L)]$$

$$\boldsymbol{\delta} = \begin{bmatrix} \theta_1 \\ \theta_1' \\ \theta_2 \\ \theta_2' \end{bmatrix}$$

Let \mathbf{G} be the vector of test functions. Using Galerkin method in which $\mathbf{G} = \mathbf{\Omega}$, the weak form can be written as

$$EI_w \int \mathbf{\Omega}''^T \mathbf{\Omega}'' \boldsymbol{\delta} dx + GJ \int \mathbf{\Omega}'^T \mathbf{\Omega}' \boldsymbol{\delta} dx = (\mathbf{\Omega}^T T)_B + (\mathbf{\Omega}'^T M_w)_B + \int \mathbf{\Omega}^T m_x dx$$

Let

$$\mathbf{k}_w = \int \mathbf{\Omega}''^T \mathbf{\Omega}'' dx \quad \text{and} \quad \mathbf{k}_s = \int \mathbf{\Omega}'^T \mathbf{\Omega}' dx$$

$$\mathbf{f} = (\boldsymbol{\Omega}^T T)_B + (\boldsymbol{\Omega}'^T M_w)_B + \int \boldsymbol{\Omega}^T m_x dx$$

Then, the element level equilibrium equation can be expressed as

$$[EI_w \mathbf{k}_w + GJ \mathbf{k}_s] \boldsymbol{\delta} = \mathbf{f}$$

Assembling the elements and imposing the boundary conditions, the nodal values of the twist angle θ can be determined. Then, the resultants T_s, T_w, M_w are computed as

$$T_s = GJ \boldsymbol{\Omega}' \boldsymbol{\delta}$$

$$T_w = -EI_w \boldsymbol{\Omega}''' \boldsymbol{\delta} \tag{3.3}$$

$$M_w = EI_w \boldsymbol{\Omega}'' \boldsymbol{\delta}$$

In this thesis, the normal and shear stress distributions over a cross section subjected to $N, M_y, M_z, S_y, S_z, T_s, T_w, M_w$ are determined.

3.2. Determination of Stresses

Triangular Finite Element

Consider a three-node finite element of area α with vertex nodes in a coordinate system yz .

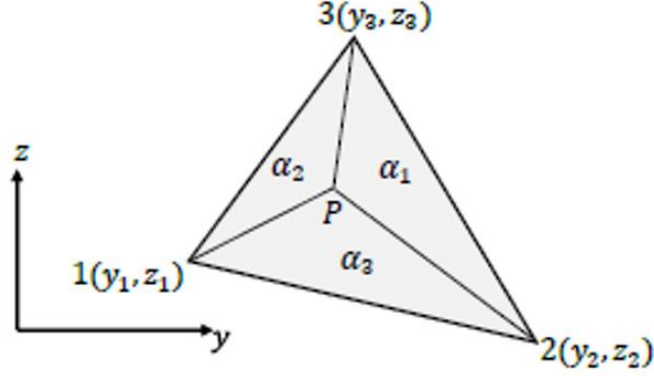


Figure 3.1: Representation of Triangular Element

The triangular coordinates are

$$\xi_i = \frac{\alpha_i}{\alpha} \quad \xi_1 + \xi_2 + \xi_3 = 1 \quad (3.4)$$

The relations between yz and

$$\begin{bmatrix} y \\ z \end{bmatrix} = \begin{bmatrix} y_1 & y_2 & y_3 \\ z_1 & z_2 & z_3 \end{bmatrix} \begin{bmatrix} \xi_1 \\ \xi_2 \\ \xi_3 \end{bmatrix} \quad \begin{bmatrix} \xi_1 \\ \xi_2 \\ \xi_3 \end{bmatrix} = \frac{1}{2\alpha} \begin{bmatrix} a_1 & b_1 \\ a_2 & b_2 \\ a_3 & b_3 \end{bmatrix} \begin{bmatrix} y \\ z \end{bmatrix} + \frac{1}{2\alpha} \begin{bmatrix} c_1 \\ c_2 \\ c_3 \end{bmatrix} \quad (3.5)$$

where

$$\begin{aligned} a_1 &= z_2 - z_3 & b_1 &= y_3 - y_2 & c_1 &= y_2 z_3 - y_3 z_2 \\ a_2 &= z_3 - z_1 & b_2 &= y_1 - y_3 & c_2 &= y_3 z_1 - y_1 z_3 \\ a_3 &= z_1 - z_2 & b_3 &= y_2 - y_1 & c_3 &= y_1 z_2 - y_2 z_1 \end{aligned} \quad (3.6)$$

For area of the triangular element

$$\alpha_1 = \frac{1}{2} (a_2 a_3 - a_3 a_2) \quad (3.7)$$

Differentiation

$$\frac{\partial}{\partial y} = \sum_{i=1}^3 a_i \frac{\partial}{\partial \xi_i} \quad \frac{\partial}{\partial z} = \sum_{i=1}^3 b_i \frac{\partial}{\partial \xi_i}$$

Note that $\xi_i = 1$ at node i and zero at nodes j and k . Then, a function $f(y, z)$ can be interpolated over a triangular domain as

$$f = \xi_1 f_1 + \xi_2 f_2 + \xi_3 f_3$$

where $f_n = f(y_n, z_n)$.

Line Integration

A function $\xi_i^I \xi_j^J$ is integrated along an edge ij of length L_{ij} as

$$\int_{ij} \xi_i^I \xi_j^J ds = L_{ij} \frac{I!J!}{(I+J+1)!} \quad (3.8)$$

Area Integration

A function $\xi_i^I \xi_j^J \xi_k^K$ is integrated over a triangle of area α as

$$\int_A \xi_i^I \xi_j^J \xi_k^K ds = 2\alpha \frac{I!J!K!}{(I+J+K+2)!} \quad (3.9)$$

Centroid, Cross-Sectional Area, Second Moments of Area

Let the section be discretized by N number of triangular elements. Let's rs be an arbitrary frame

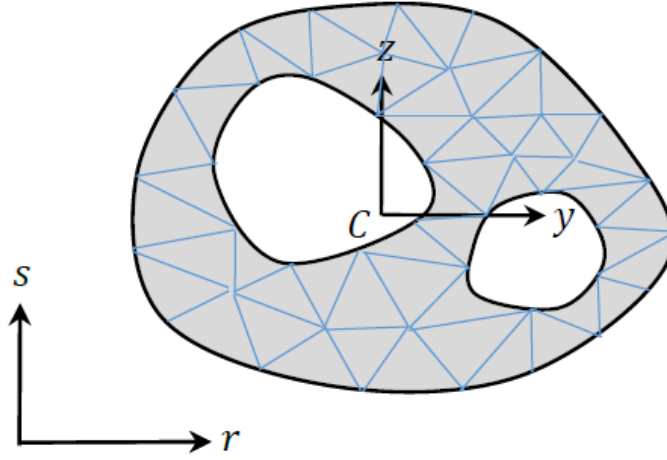


Figure 3.2: yz and rs Coordinates Frame

The cross-sectional area is

$$A = \sum_{n=1}^N \alpha_n = \frac{1}{2} \sum_{n=1}^N (a_2 b_3 - a_3 b_2)_n \quad (3.10)$$

Note that

$$\int_A r dA = \sum_{n=1}^N \int (r_1 \xi_1 + r_2 \xi_2 + r_3 \xi_3)_n dA = \frac{1}{3} \sum_{n=1}^N \alpha_n (r_1 + r_2 + r_3)_n$$

$$\int_A s dA = \sum_{n=1}^N \int (s_1 \xi_1 + s_2 \xi_2 + s_3 \xi_3)_n dA = \frac{1}{3} \sum_{n=1}^N \alpha_n (s_1 + s_2 + s_3)_n$$

Then, the coordinates of the centroid $C(\bar{r}, \bar{s})$ are

$$\bar{r} = \frac{1}{A} \int_A r dA = \frac{1}{3A} \sum_{n=1}^N \alpha_n (r_1 + r_2 + r_3)_n$$

$$\bar{s} = \frac{1}{A} \int_A s dA = \frac{1}{3A} \sum_{n=1}^N \alpha_n (s_1 + s_2 + s_3)_n$$

Let yz be a centroidal frame parallel to rs . Then

$$y = r - \bar{r} \quad z = s - \bar{s}$$

And the second moments of area are defined as

$$\begin{aligned} I_y &= \int_A z^2 dA = \sum_{n=1}^N \int_{\alpha_n} (z_1 \xi_1 + z_2 \xi_2 + z_3 \xi_3)_n^2 dA \\ &= \frac{1}{6} \sum_{n=1}^N \alpha_n (z_1^2 + z_2^2 + z_3^2 + z_1 z_2 + z_2 z_3 + z_3 z_1)_n \end{aligned} \quad (3.11a)$$

$$\begin{aligned} I_z &= \int_A y^2 dA = \sum_{n=1}^N \int_{\alpha_n} (y_1 \xi_1 + y_2 \xi_2 + y_3 \xi_3)_n^2 dA \\ &= \frac{1}{6} \sum_{n=1}^N \alpha_n (y_1^2 + y_2^2 + y_3^2 + y_1 y_2 + y_2 y_3 + y_3 y_1)_n \end{aligned} \quad (3.11b)$$

$$\begin{aligned} I_{yz} &= - \int_A yz dA = - \sum_{n=1}^N \int_{\alpha_n} (y_1 \xi_1 + y_2 \xi_2 + y_3 \xi_3)_n (z_1 \xi_1 + z_2 \xi_2 + z_3 \xi_3)_n dA \\ &= - \sum_{n=1}^N \alpha_n \left[\frac{1}{6} (y_1 z_1 + y_2 z_2 + y_3 z_3)_n \right. \\ &\quad \left. + \frac{1}{12} (y_1 z_2 + y_2 z_1 + y_2 z_3 + y_3 z_2 + y_3 z_1 + y_1 z_3)_n \right] \end{aligned} \quad (3.11c)$$

Divergence Theorem

Consider a beam section in the yz plane. Let A be the area and B be the boundary of the cross section. The boundary B consists of the outer boundary B_O and the inner boundaries $B_i (i = 1, \dots, n)$. Along each boundary, a set of coordinates ns is defined such that s is tangent to boundary, n is normal to the boundary and xns is a right-handed coordinate system. $\mathbf{n} = n_y \mathbf{j} + n_z \mathbf{k}$ is the unit vector in the direction n .

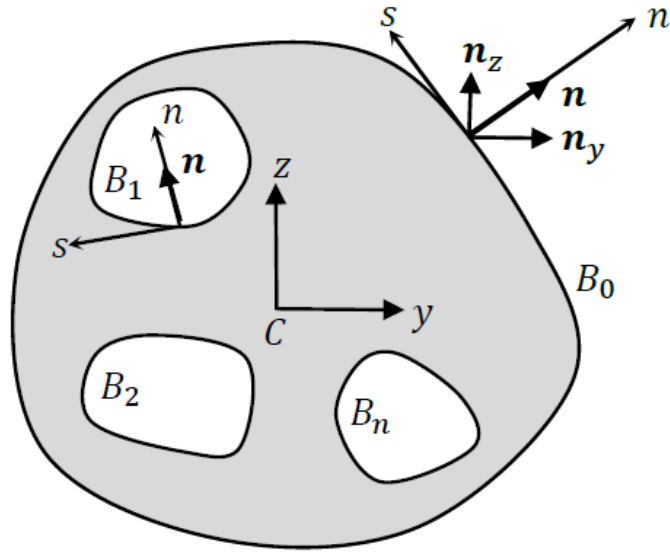


Figure 3.3: Normal Vectors in Arbitrary Cross Section

Let $\mathbf{F} = F_y \mathbf{j} + F_z \mathbf{k}$ be a vector function. Then,

$$\int_A \nabla \cdot \mathbf{F} dA = \int_B \mathbf{F} \cdot \mathbf{n} ds$$

where

$$\nabla = \frac{\partial}{\partial y} \mathbf{j} + \frac{\partial}{\partial z} \mathbf{k}$$

Let $g(y, z)$ be a scalar function. Then,

$$\int_A \nabla \cdot g \mathbf{F} dA = \int_B g \mathbf{F} \cdot \mathbf{n} ds$$

Note that

$$\begin{aligned} \nabla \cdot g \mathbf{F} &= \left(\frac{\partial}{\partial y} \mathbf{j} + \frac{\partial}{\partial z} \mathbf{k} \right) (g F_y \mathbf{j} + g F_z \mathbf{k}) = \frac{\partial}{\partial y} (g F_y) + \frac{\partial}{\partial z} (g F_z) \\ &= F_y \frac{\partial g}{\partial y} + g \frac{\partial F_y}{\partial y} + F_z \frac{\partial g}{\partial z} + g \frac{\partial F_z}{\partial z} = g \left(\frac{\partial F_y}{\partial y} + \frac{\partial F_z}{\partial z} \right) + \left(F_y \frac{\partial g}{\partial y} + F_z \frac{\partial g}{\partial z} \right) \end{aligned}$$

$$\begin{aligned}
&= g \left(\frac{\partial}{\partial y} \mathbf{j} + \frac{\partial}{\partial z} \mathbf{k} \right) \cdot (F_y \mathbf{j} + F_z \mathbf{k}) + \left(\frac{\partial g}{\partial y} \mathbf{j} + \frac{\partial g}{\partial z} \mathbf{k} \right) \cdot (F_y \mathbf{j} + F_z \mathbf{k}) \\
&= g \nabla \cdot \mathbf{F} + \nabla g \cdot \mathbf{F}
\end{aligned}$$

Then,

$$\int_A (g \nabla \cdot \mathbf{F} + \nabla g \cdot \mathbf{F}) dA = \int_B g \mathbf{F} \cdot \mathbf{n} ds \rightarrow \int_A g \nabla \cdot \mathbf{F} dA = \int_B g \mathbf{F} \cdot \mathbf{n} ds - \int_A \nabla g \cdot \mathbf{F} dA$$

Let $\mathbf{F} = \nabla f$ where $f = f(y, z)$ is a scalar function. Then,

$$\begin{aligned}
\int_A g \nabla \cdot \nabla f dA &= \int_B g \nabla f \cdot \mathbf{n} ds - \int_A \nabla g \cdot \nabla f dA \\
\rightarrow \int_A g \nabla^2 f dA &= \int_B g \nabla f \cdot \mathbf{n} ds - \int_A \nabla g \cdot \nabla f dA
\end{aligned}$$

Consider N number of functions $g_n (n = 1, \dots, N)$. Let

$$\mathbf{g} = [g_1(y, z) \quad g_1(y, z) \quad \dots \quad g_N(y, z)]$$

Then,

$$\int_A \mathbf{g}^T \nabla^2 f dA = \int_B \mathbf{g}^T \nabla f \cdot \mathbf{n} ds - \int_A \nabla \mathbf{g}^T \cdot \nabla f dA \tag{3.12}$$

3.2.1. Stresses due to Normal Force and Bending Moments

The normal stress due to axial force N and bending moments M_y and M_z is

$$\sigma_{xx} = \frac{N}{A} + \frac{1}{(I_y I_z - I_{yz}^2)} [M_y (I_{zz} z + I_{yz} y) - M_z (I_{yy} z + I_{yz} y)] \quad (3.13)$$

3.2.2. Stresses due to Shear Forces

Consider a beam cross section in the yz plane. Let the shear forces S_y and S_z act through the shear center O . Therefore, there is no twisting in the section. The stresses on the section are the normal stress σ_x and the shear stresses τ_{xy} and τ_{xz} . The equilibrium requires that

$$\frac{\partial \sigma_{xx}}{\partial x} + \frac{\partial \tau_{xy}}{\partial y} + \frac{\partial \tau_{xz}}{\partial z} = 0$$

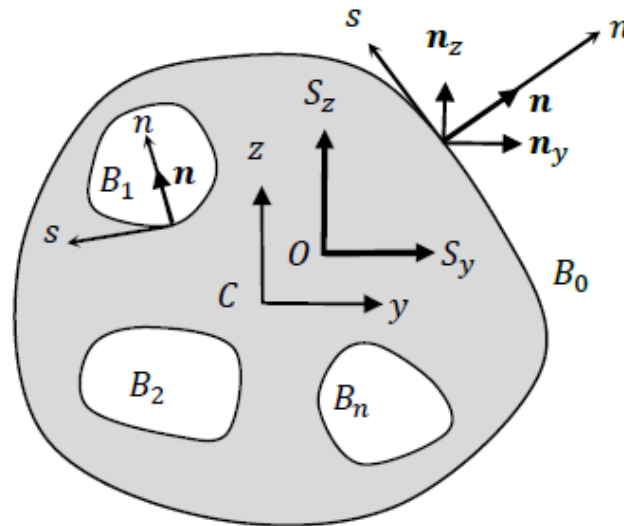


Figure 3.4: Shear Center and Centroid in Arbitrary Cross Section

Noting that

$$\sigma_{xx} = \frac{1}{(I_{yy} I_{zz} - I_{yz}^2)} [M_y (I_{zz} z + I_{yz} y) - M_z (I_{yy} z + I_{yz} y)]$$

$$M'_y = S_z$$

$$M'_z = S_y$$

we get

$$\frac{\partial \tau_{xy}}{\partial y} + \frac{\partial \tau_{xz}}{\partial z} = -h(y, z)$$

where

$$h(y, z) = \frac{1}{(I_{yy}I_{zz} - I_{yz}^2)} [S_y(I_{zz}z + I_{yz}y) + S_z(I_{yy}z + I_{yz}y)] \quad (3.14)$$

Let $\varphi(y, z)$ be a stress function such that

$$\tau_{xy} = \frac{\partial \varphi}{\partial y} \quad \text{and} \quad \tau_{xz} = \frac{\partial \varphi}{\partial z}$$

Then, the governing equation is obtained by substituting eq. (2) and eq. (3) into eq. (4)

$$\frac{\partial^2 \varphi}{\partial y^2} + \frac{\partial^2 \varphi}{\partial z^2} = -h(y, z) \rightarrow \nabla^2 \varphi + h = 0$$

The Cauchy's relation can be written on the boundaries as

$$\begin{bmatrix} \sigma_{xx} & \tau_{xy} & \tau_{xz} \\ \tau_{xy} & 0 & 0 \\ \tau_{xz} & 0 & 0 \end{bmatrix} \begin{bmatrix} 0 \\ n_y \\ n_z \end{bmatrix} = \begin{bmatrix} 0 \\ 0 \\ 0 \end{bmatrix}$$

noting that the outer and inner boundaries of the beam are stress free. The second and third rows are identically satisfied. The first row gives

$$\tau_{xy}n_y + \tau_{xz}n_z = 0$$

which can be written as

$$\frac{\partial \varphi}{\partial y} n_y + \frac{\partial \varphi}{\partial z} n_z = 0 \rightarrow \left[\frac{\partial \varphi}{\partial y} \quad \frac{\partial \varphi}{\partial z} \right] \begin{bmatrix} n_y \\ n_z \end{bmatrix} = 0 \rightarrow \nabla \varphi \cdot \mathbf{n} = 0 \text{ for } B_i \ (i = 0, 1, \dots, N)$$

This condition applies to both outer and inner boundaries.

The weak form is

$$\int_A g(\nabla^2 \varphi + h) dA = 0$$

Consider N number of functions $g_n \ (n = 1, \dots, N)$. Let

$$\mathbf{g} = [g_1(y, z) \quad g_1(y, z) \quad \dots \quad g_N(y, z)]$$

Then,

$$\int_A \mathbf{g}^T (\nabla^2 \varphi + h) dA = 0 \xrightarrow{\text{rearranging}} \int_A \mathbf{g}^T \nabla^2 \varphi dA = - \int_A \mathbf{g}^T h dA$$

Using the Green-Gauss Theorem,

$$\int_A \mathbf{g}^T \cdot \nabla^2 \varphi dA = \int_B \mathbf{g}^T \nabla \varphi \cdot \mathbf{n} ds - \int_A \nabla \mathbf{g}^T \cdot \nabla \varphi dA$$

Then, the weak form can be written as

$$\int_A \nabla \mathbf{g}^T \cdot \nabla \varphi dA = \int_B \mathbf{g}^T \nabla \varphi \cdot \mathbf{n} ds - \int_A \mathbf{g}^T h dA$$

The first integral on the right-hand side is zero due to the boundary condition $\nabla \varphi \cdot \mathbf{n} = 0$. Then, the weak form is

$$\int_A \nabla \mathbf{g}^T \cdot \nabla \varphi dA = \int_A \mathbf{g}^T h dA$$

The solution of the equation (7) is carried out with the finite element formulations.

Finite Element Formulation

Assume the stress function within the n^{th} element as

$$\varphi = [\xi_1 \quad \xi_2 \quad \xi_3] \begin{bmatrix} \varphi_1 \\ \varphi_2 \\ \varphi_3 \end{bmatrix} = \mathbf{P} \mathbf{q}$$

Then,

$$\nabla \varphi = \nabla \mathbf{P} \mathbf{q} = \begin{bmatrix} \frac{\partial}{\partial x} \\ \frac{\partial}{\partial y} \\ \frac{\partial}{\partial z} \end{bmatrix} [\xi_1 \quad \xi_2 \quad \xi_3] \begin{bmatrix} \varphi_1 \\ \varphi_2 \\ \varphi_3 \end{bmatrix} = \begin{bmatrix} \frac{\partial \xi_1}{\partial x} & \frac{\partial \xi_2}{\partial x} & \frac{\partial \xi_3}{\partial x} \\ \frac{\partial \xi_1}{\partial y} & \frac{\partial \xi_2}{\partial y} & \frac{\partial \xi_3}{\partial y} \\ \frac{\partial \xi_1}{\partial z} & \frac{\partial \xi_2}{\partial z} & \frac{\partial \xi_3}{\partial z} \end{bmatrix} \begin{bmatrix} \varphi_1 \\ \varphi_2 \\ \varphi_3 \end{bmatrix}$$

$$\mathbf{B} \mathbf{q} = \frac{1}{2A} \begin{bmatrix} a_1 & a_2 & a_3 \\ b_1 & b_2 & b_3 \end{bmatrix} \begin{bmatrix} \varphi_1 \\ \varphi_2 \\ \varphi_3 \end{bmatrix}$$

In Galerkin method, the test functions are chosen that

$$\mathbf{g} = \frac{\partial \varphi}{\partial \mathbf{q}} \rightarrow \mathbf{g} = \mathbf{P} \rightarrow \nabla \mathbf{g} = \nabla \mathbf{P} = \mathbf{B}$$

Then, the weak form can be written for a finite element as

$$\int_A \mathbf{B}^T \mathbf{B} \mathbf{q} dA = \int_A \mathbf{P}^T h dA$$

Then, the element level equilibrium equations are

$$\mathbf{k} \mathbf{q} = \mathbf{f}$$

where

$$\begin{aligned} \mathbf{k} &= \int_{\alpha} \mathbf{B}^T \mathbf{B} dA \\ &= \frac{1}{4\alpha} \begin{bmatrix} (a_1 a_1 + b_1 b_1) & (a_1 a_2 + b_1 b_2) & (a_1 a_3 + b_1 b_3) \\ (a_2 a_1 + b_2 b_1) & (a_2 a_2 + b_2 b_2) & (a_2 a_3 + b_2 b_3) \\ (a_3 a_1 + b_3 b_1) & (a_3 a_2 + b_3 b_2) & (a_3 a_3 + b_3 b_3) \end{bmatrix} \end{aligned} \quad (3.15)$$

$$\begin{aligned} \mathbf{f} &= \int_{\alpha} \mathbf{P}^T h dA \\ &= \frac{S_y}{I_{yy} I_{zz} - I_{yz}^2} \int_{\alpha} P^T (I_{yy} y + I_{yz} z) dA + \frac{S_z}{I_{yy} I_{zz} - I_{yz}^2} \int_{\alpha} P^T (I_{zz} z + I_{yz} y) dA \\ &= \frac{A}{12(I_{yy} I_{zz} - I_{yz}^2)} \begin{bmatrix} 2 & 1 & 1 \\ 1 & 2 & 1 \\ 1 & 1 & 2 \end{bmatrix} \left[(S_y I_{yy} + S_z I_{yz}) \begin{bmatrix} y_1 \\ y_2 \\ y_3 \end{bmatrix} + (S_z I_{zz} + S_y I_{yz}) \begin{bmatrix} z_1 \\ z_2 \\ z_3 \end{bmatrix} \right] \end{aligned} \quad (3.16)$$

As a result, the shear stresses in the element due to shear force S are calculated as

$$\begin{bmatrix} \tau_{xy} \\ \tau_{xz} \end{bmatrix} = \mathbf{B} \mathbf{q} = \frac{1}{2A} \begin{bmatrix} a_1 & a_2 & a_3 \\ b_1 & b_2 & b_3 \end{bmatrix} \begin{bmatrix} \varphi_1 \\ \varphi_2 \\ \varphi_3 \end{bmatrix} \quad (3.17)$$

Shear Center

The torque created by τ_{xy} and τ_{xz} is

$$\begin{aligned} T &= \int_A (\tau_{xz} y - \tau_{xy} z) dA = \sum_{n=1}^N A_n [(\tau_{xz})_n \bar{y}_n - (\tau_{xy})_n \bar{z}_n] \\ &= \frac{1}{3} \sum_{n=1}^N \alpha_n [\tau_{xz} (y_1 + y_2 + y_3) - \tau_{xy} (z_1 + z_2 + z_3)]_n \end{aligned} \quad (3.18)$$

Nothing that, for the present three-node element, the shear stresses τ_{xy} and τ_{xz} are constant over the element. The shear center $O(y_0, z_0)$ is a point in the cross-sectional plane such that the shear forces acting through it do not cause twisting of the section. Then, y_0 is determined by taking $S_z \neq 0$ and $S_y = 0$, and z_0 is determined by taking $S_y \neq 0$ and $S_z = 0$ as

$$y_0 = \frac{T}{S_z} \text{ and } z_0 = -\frac{T}{S_y} \quad (3.19)$$

The shear center is also the twist center about which a section rotates under the action of a torque.

3.2.3. Stresses due to Saint Venant's Torque

Consider uniform torsion such that θ' is constant and $\theta = \theta' x$. In this situation, torque and angle of twist rate are constant along the beam. In addition, the warping displacement is dependent of y and z coordinates, and independent of x coordinate.

Then, the displacements are

$$\begin{aligned} u &= \tilde{\omega}\theta' \\ v &= -(z - z_0)\theta' \\ w &= (y - y_0)\theta' \end{aligned} \quad (3.20)$$

where $\tilde{\omega}(y, z)$ is the warping function. Then, the nonzero strains and stresses are

$$\begin{aligned} \gamma_{xy} &= \theta' \left(\frac{\partial \tilde{\omega}}{\partial y} - z + z_0 \right) & \gamma_{xz} &= \theta' \left(\frac{\partial \tilde{\omega}}{\partial z} + y - y_0 \right) \\ \tau_{xy} &= G\gamma_{xy} = G\theta' \left(\frac{\partial \tilde{\omega}}{\partial y} - z + z_0 \right) & \tau_{xz} &= G\gamma_{xz} = G\theta' \left(\frac{\partial \tilde{\omega}}{\partial z} + y - y_0 \right) \end{aligned}$$

Then, St. Venant torque is defined as

$$T_s = \int_A (\tau_{xz}y - \tau_{xy}z) dA = GJ\theta'$$

where

$$J = \int_A \left[(y - y_0) \frac{\partial \tilde{\omega}}{\partial z} - (z - z_0) \frac{\partial \tilde{\omega}}{\partial y} + (y - y_0)^2 + (z - z_0)^2 \right] dA$$

$$= I_y + I_z + A(y_0^2 + z_0^2) + \int_A \left[(y - y_0) \frac{\partial \tilde{\omega}}{\partial z} - (z - z_0) \frac{\partial \tilde{\omega}}{\partial y} \right] dA$$

is the torsional constant of the section.

The equilibrium condition gives

$$\frac{\partial \tau_{xy}}{\partial y} + \frac{\partial \tau_{xz}}{\partial z} = 0 \rightarrow \frac{\partial^2 \tilde{\omega}}{\partial y^2} + \frac{\partial^2 \tilde{\omega}}{\partial z^2} = 0$$

Thus, the governing equation is obtained as $\nabla^2 \tilde{\omega} = 0$

Cauchy's relation gives the boundary conditions as

$$\left(\frac{\partial \tilde{\omega}}{\partial y} - z + z_0 \right) n_y + \left(\frac{\partial \tilde{\omega}}{\partial z} + y - y_0 \right) n_z = 0$$

$$\rightarrow \left(\frac{\partial \tilde{\omega}}{\partial y} \right) n_y + \left(\frac{\partial \tilde{\omega}}{\partial z} \right) n_z = (z - z_0) n_y - (y - y_0) n_z$$

Let $\lambda = (z - z_0) n_y - (y - y_0) n_z$

Then, boundary condition is $\nabla \tilde{\omega} \cdot \mathbf{n} = \lambda$

This condition must be satisfied along external and internal boundaries B_i ($i = 0, 1, \dots, N$)

The weak form is obtained by using the governing equation as

$$\int_A \mathbf{g}^T \nabla^2 \tilde{\omega} dA = 0$$

Using the divergence theorem

$$\int_A \mathbf{g}^T \nabla^2 \tilde{\omega} dA = \int_B \mathbf{g}^T \nabla \tilde{\omega} \cdot \mathbf{n} dS - \int_A \nabla \mathbf{g}^T \cdot \nabla \tilde{\omega} dA = \int_B \mathbf{g}^T \lambda dS - \int_A \nabla \mathbf{g}^T \cdot \nabla \tilde{\omega} dA$$

Then, the weak form becomes

$$\int_A \nabla \mathbf{g}^T \cdot \nabla \tilde{\omega} dA = \int_A \mathbf{g}^T \lambda dS$$

Finite Element Formulation

Assume the warping function within an element as

$$\tilde{\omega} = \mathbf{P} \mathbf{q} = [\xi_1 \quad \xi_2 \quad \xi_3] \begin{bmatrix} \tilde{\omega}_1 \\ \tilde{\omega}_2 \\ \tilde{\omega}_3 \end{bmatrix}$$

Then,

Recall that $\mathbf{g} = \mathbf{P} \rightarrow \nabla \mathbf{g} = \nabla \mathbf{P} = \mathbf{B}$. Then, the weak form can be written for a finite element as

$$\int_{\alpha} \mathbf{B}^T \mathbf{B} \mathbf{q} dA = \int_{\beta} \mathbf{P}^T \lambda dS$$

where β denotes the element boundary. Then, the element level equilibrium equations are $\mathbf{k} \mathbf{q} = \mathbf{f}$

where

$$\mathbf{k} = \int_{\alpha} [\mathbf{B}]^T \mathbf{B} dA$$

$$= \frac{1}{4\alpha} \begin{bmatrix} (a_1 a_1 + b_1 b_1) & (a_1 a_2 + b_1 b_2) & (a_1 a_3 + b_1 b_3) \\ (a_2 a_1 + b_2 b_1) & (a_2 a_2 + b_2 b_2) & (a_2 a_3 + b_2 b_3) \\ (a_3 a_1 + b_3 b_1) & (a_3 a_2 + b_3 b_2) & (a_3 a_3 + b_3 b_3) \end{bmatrix} \quad (3.21)$$

The force vector can be expressed as

$$\mathbf{f} = \mathbf{f}_{12} + \mathbf{f}_{23} + \mathbf{f}_{31} \quad (3.22)$$

where f_{ij} is the force vector related with the edge ij . Note that the normal vector components for the edge ij are

$$n_y = \frac{(z_j - z_i)}{L_{ij}} \quad n_z = \frac{(y_j - y_i)}{L_{ij}}$$

Then, f_{ij} can be evaluated as follows:

If the edge-12 is not on the boundary, then

$$f_{12} = \begin{bmatrix} 0 \\ 0 \\ 0 \end{bmatrix}$$

If the edge-12 is on the boundary, then

$$f_{12} = \frac{1}{L_{12}} \int_{12} \begin{bmatrix} \xi_1 \\ \xi_2 \\ 0 \end{bmatrix} [(z_1 \xi_1 + z_2 \xi_2 - z_0)(z_2 - z_1) + (y_1 \xi_1 + y_2 \xi_2 - y_0)(y_2 - y_1)] ds$$

If the edge-23 is not on the boundary, then

$$f_{23} = \begin{bmatrix} 0 \\ 0 \\ 0 \end{bmatrix}$$

If the edge-23 is on the boundary, then

$$f_{23} = \frac{1}{L_{23}} \int_{23} \begin{bmatrix} 0 \\ \xi_2 \\ \xi_3 \end{bmatrix} [(z_2 \xi_2 + z_3 \xi_3 - z_0)(z_3 - z_2) + (y_2 \xi_2 + y_3 \xi_3 - y_0)(y_3 - y_2)] ds$$

If the edge-31 is not on the boundary, then

$$f_{31} = \begin{bmatrix} 0 \\ 0 \\ 0 \end{bmatrix}$$

If the edge-31 is on the boundary, then

$$f_{31} = \frac{1}{L_{31}} \int_{31} \begin{bmatrix} \xi_1 \\ 0 \\ \xi_3 \end{bmatrix} [(z_3 \xi_3 + z_1 \xi_1 - z_0)(z_1 - z_3) + (y_3 \xi_3 + y_1 \xi_1 - y_0)(y_1 - y_3)] ds$$

Define

$$\bar{\omega} = \frac{1}{A} \int_A \tilde{\omega} dA = \frac{1}{A} \sum_{n=1}^N \int_{\alpha_n} [\xi_1 \quad \xi_2 \quad \xi_3] \begin{bmatrix} \tilde{\omega}_1 \\ \tilde{\omega}_2 \\ \tilde{\omega}_3 \end{bmatrix} dA = \frac{1}{3A} \sum_{n=1}^N \alpha_n (\tilde{\omega}_1 + \tilde{\omega}_2 + \tilde{\omega}_3)_n$$

Then, the warping function is normalized as $\omega = \tilde{\omega} - \bar{\omega}$. And, $\tilde{\omega}$ is replaced by ω in all equations. Note that, within a finite element

$$\begin{bmatrix} \frac{\partial \omega}{\partial y} \\ \frac{\partial \omega}{\partial z} \end{bmatrix} = \nabla \omega = \mathbf{B} \mathbf{q} \rightarrow \begin{bmatrix} \frac{\partial \omega}{\partial y} & \frac{\partial \omega}{\partial z} \end{bmatrix} = \mathbf{q}^T \mathbf{B}^T$$

Then, for a section discretized by N number of finite elements, J can be expressed as

$$\begin{aligned} J &= I_{yy} + I_{zz} + A(y_0^2 + z_0^2) + \int_A \left[(y - y_0) \frac{\partial \omega}{\partial z} - (z - z_0) \frac{\partial \omega}{\partial y} \right] dA \\ &= I_{yy} + I_{zz} + A(y_0^2 + z_0^2) + \sum_{n=1}^N \int_{A_n} \left[\mathbf{q}^T \mathbf{B}^T \begin{bmatrix} z_0 - z \\ y - y_0 \end{bmatrix} \right] dA \\ &= I_{yy} + I_{zz} + A(y_0^2 + z_0^2) \\ &\quad + \frac{1}{6} \sum_{n=1}^N [\omega_1 \quad \omega_2 \quad \omega_3] \begin{bmatrix} a_1 & b_1 \\ a_2 & b_2 \\ a_3 & b_3 \end{bmatrix} \begin{bmatrix} 3z_0 - z_1 - z_2 - z_3 \\ y_1 + y_2 + y_3 - 3y_0 \end{bmatrix} \end{aligned} \quad (3.23)$$

The shear stresses at point (y, z) in an element due to St. Venant torque T_s are evaluated as

$$\begin{aligned}
\begin{bmatrix} \tau_{xy} \\ \tau_{xz} \end{bmatrix} &= G\theta' \begin{bmatrix} \frac{\partial \omega}{\partial y} - z + z_0 \\ \frac{\partial \omega}{\partial z} + y - y_0 \end{bmatrix} = G\theta' \left[\mathbf{B}\mathbf{q} + \begin{bmatrix} z_0 - z \\ y - y_0 \end{bmatrix} \right] = \frac{T_S}{J} \left[\mathbf{B}\mathbf{q} + \begin{bmatrix} z_0 - z \\ y - y_0 \end{bmatrix} \right] \\
&= \frac{T_S}{J} \left[\frac{1}{2A} \begin{bmatrix} a_1 & a_2 & a_3 \\ b_1 & b_2 & b_3 \end{bmatrix} \begin{bmatrix} \omega_1 \\ \omega_2 \\ \omega_3 \end{bmatrix} + \begin{bmatrix} z_0 - z \\ y - y_0 \end{bmatrix} \right]
\end{aligned} \tag{3.24}$$

3.2.4. Stresses due to Warping Torque and Warping Moment

If $\theta' = \theta'(x)$, then the torsion is non-uniform. In this situation, torque and angle of twist rate is not constant along the beam. Furthermore, the warping displacement is dependent of x, y, and z coordinates.

The normal stress in the warping is

$$\sigma_x = E\omega\theta'''$$

The warping moment M_w and warping torque T_w are defined as

$$M_w = \int_A \sigma_x \omega t ds = EI_w \theta''$$

$$T_w = -M_w = -EI_w \theta'''$$

Then, the normal stress due to warping moment M_w is

$$\sigma_x = \frac{M_w}{I_w} (\omega_n)_{ave} \quad \text{where} \quad (\omega_n)_{ave} = \frac{\omega_1 + \omega_2 + \omega_3}{3} \tag{3.25}$$

The equilibrium requires that

$$\frac{\partial \tau_{xy}}{\partial y} + \frac{\partial \tau_{xz}}{\partial z} + \frac{\partial \sigma_{xx}}{\partial x} = 0 \rightarrow \frac{\partial \tau_{xy}}{\partial y} + \frac{\partial \tau_{xz}}{\partial z} = -\frac{\partial \sigma_{xx}}{\partial x} = -E\omega\theta''' = \frac{T_w}{I_w} \omega$$

Let $\phi(y, z)$ be a stress function such that

$$\tau_{xy} = \frac{\partial \phi}{\partial y} \quad \text{and} \quad \tau_{xz} = \frac{\partial \phi}{\partial z}$$

Then, the governing equation is obtained as

$$\frac{\partial^2 \phi}{\partial y^2} + \frac{\partial^2 \phi}{\partial z^2} = \frac{T_w}{I_w} \omega \rightarrow \nabla^2 \phi - \frac{T_w}{I_w} \omega = 0$$

The Cauchy's relation can be written on the boundaries as

$$\tau_{xy}n_y + \tau_{xz}n_z = 0 \rightarrow \nabla \phi \cdot \mathbf{n} = 0$$

This boundary condition applies to both outer and inner boundaries. Then, the weak form is

$$\int_A \mathbf{g}^T \left(\nabla^2 \phi - \frac{T_w}{I_w} \omega \right) dA = 0 \rightarrow \int_A \mathbf{g}^T \nabla^2 \phi dA - \int_A \mathbf{g}^T \frac{T_w}{I_w} \omega dA = 0$$

Using the Green-Gauss theorem and imposing the boundary conditions

$$\int_A \mathbf{g}^T \nabla^2 \phi dA = \int_B \mathbf{g}^T \nabla \phi \cdot \mathbf{n} dS - \int_A \nabla \mathbf{g}^T \cdot \nabla \phi dA = \int_A \nabla \mathbf{g}^T \cdot \nabla \phi dA$$

Then, the weak form is

$$\int_A \nabla \mathbf{g}^T \cdot \nabla \phi dA = - \frac{T_w}{I_w} \int_A \mathbf{g}^T \omega dA = 0$$

Finite Element Formulation

Assume the stress function within an element as

$$\phi = \mathbf{P}\mathbf{q} = [\xi_1 \quad \xi_2 \quad \xi_3] \begin{bmatrix} \phi_1 \\ \phi_2 \\ \phi_3 \end{bmatrix}$$

Then,

$$\nabla \phi = \nabla \mathbf{P}\mathbf{q} = \frac{1}{2A} \begin{bmatrix} a_1 & a_2 & a_3 \\ b_1 & b_2 & b_3 \end{bmatrix} \begin{bmatrix} \phi_1 \\ \phi_2 \\ \phi_3 \end{bmatrix} = \mathbf{B}\mathbf{q}$$

Recall that $\nabla \mathbf{g} = \nabla \mathbf{P} = \mathbf{B}$. Then, the weak form can be written for a finite element as

$$\int_{\alpha} \mathbf{B}^T \mathbf{B} \mathbf{q} dA = -\frac{T_w}{I_w} \int_{\alpha} \mathbf{P}^T \omega dA$$

Then, the element level equilibrium equations are $\mathbf{kq} = \mathbf{f}$

$$\mathbf{k} = \int_{\alpha} \mathbf{B}^T \mathbf{B} dA = \frac{1}{4\alpha} \begin{bmatrix} (a_1 a_1 + b_1 b_1) & (a_1 a_2 + b_1 b_2) & (a_1 a_3 + b_1 b_3) \\ (a_2 a_1 + b_2 b_1) & (a_2 a_2 + b_2 b_2) & (a_2 a_3 + b_2 b_3) \\ (a_3 a_1 + b_3 b_1) & (a_3 a_2 + b_3 b_2) & (a_3 a_3 + b_3 b_3) \end{bmatrix} \quad (3.26)$$

$$\mathbf{f} = -\frac{T_w}{I_w} \int_{\alpha} \mathbf{P}^T \omega dA = \frac{\alpha T_w}{12 I_w} \begin{bmatrix} 2 & 1 & 1 \\ 1 & 2 & 1 \\ 1 & 1 & 2 \end{bmatrix} \begin{bmatrix} \omega_1 \\ \omega_2 \\ \omega_3 \end{bmatrix} \quad (3.27)$$

The shear stresses in an element due to warping torque T_w can be calculated as

$$\begin{bmatrix} \tau_{xy} \\ \tau_{xz} \end{bmatrix} = \begin{bmatrix} \frac{\partial \phi}{\partial y} \\ \frac{\partial \phi}{\partial z} \end{bmatrix} = \nabla \phi = \mathbf{B} \mathbf{q} = \frac{1}{2\alpha} \begin{bmatrix} a_1 & a_2 & a_3 \\ b_1 & b_2 & b_3 \end{bmatrix} \begin{bmatrix} \phi_1 \\ \phi_2 \\ \phi_3 \end{bmatrix} \quad (3.28)$$

CHAPTER 4

NUMERICAL EXAMPLES

4.1. Solid Sections

4.1.1. Rail Section

An A100 Crane Rail is a type of crane used for railroads. It can be exposed to different loadings such as transversal and torsional forces. In this example, the rail section is subjected to the shear force in the negative z-direction. The problem is compared with the German code DIN 536 Design Specification [28], and the article “Shear Stresses in Prismatic Beams with Arbitrary Cross-Sections” [20]. The cross-section properties are matched with said German design specifications [28], and the warping function, shear stress, and shear flows are checked with the aforementioned article by F. Gruttmann, R. Sauer, and W. Wagner [20]. In Figure 4.1, the loading type and meshed geometry are shown. The cross section is discretized by 1791 elements. The geometrical data for an A100 Crane Rail is given in Appendix A.1.



Figure 4.1: Loading Type and Meshed Geometry for the Rail Section

In Table 4.1, the warping constant among cross-section properties is compared with the article [20] while other parameters are tested with the DIN 536 Design Specifications [28] since the warping constant is not available in the said article.

Table 4.1: Comparison of Cross-section Properties for the Rail Section

Property Name	Present Study	Article and DIN 536	Error (%)
Area (mm ²)	0.95013E+04	0.94700E+04	0.33
Centroid, y_c (mm)	0.00000E+00	0.00000E+00	0.00
Centroid, z_c (mm)	0.42477E+02	0.42100E+02	0.89
Shear Center, y_s (mm)	0.00000E+00	0.00000E+00	0.00
Shear Center, z_s (mm)	-0.98812E+01	-0.98000E+01	0.82
Inertia, I_{yy} (mm)	0.86852E+07	0.85600E+07	1.44
Inertia, I_{zz} (mm)	0.13378E+08	0.13450E+08	0.54
Torsional Constant (mm ⁴)	0.67555E+07	0.67070E+07	0.72
Warping Constant (mm ⁶)	0.39299E+10	0.39940E+10	1.63

Having done the comparison of the cross-section parameters, the rail is analyzed under shear force. In Figure 4.2, the distribution of the shear flows is shown. They have higher intensity in the middle corner regions. According to Figure 4.3, the article [20] obtains the maximum shear stress value as -0.41 MPa. Likewise, the study conducted herein resulted in -0.39 MPa. As seen in the figure, the upper and lower zones are stress-free.

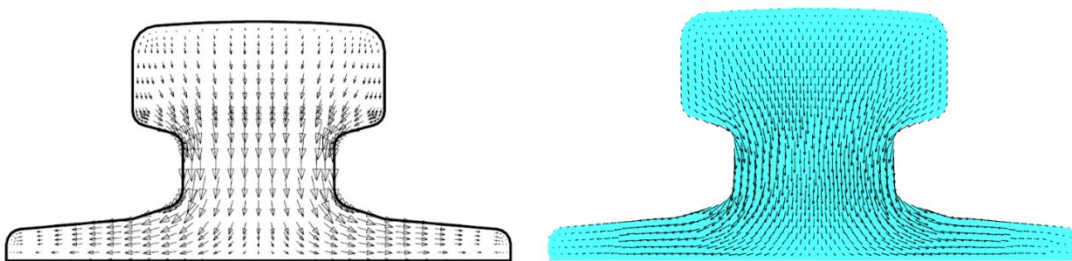


Figure 4.2: Comparison of Shear Flows for the Rail Section

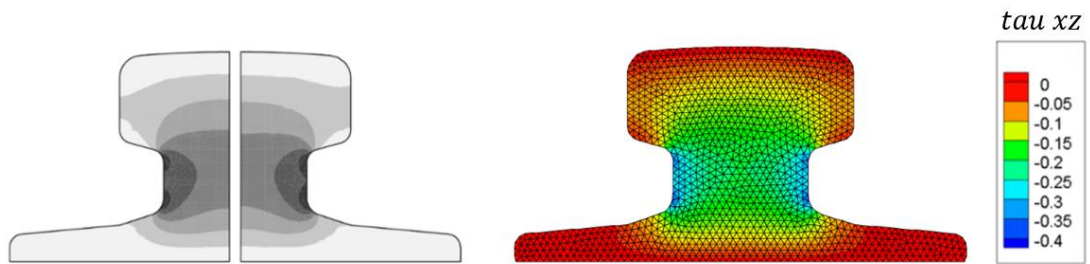


Figure 4.3: Comparison of the Shear Stresses for the Rail Section (MPa)

Lastly, the warping function is plotted in Figure 4.4. At its maximum value, the article [20] obtains 1888 mm^2 , and the study conducted for this thesis results in 1889 mm^2 . As seen in the figure, the cross-section warps at the corner zones.

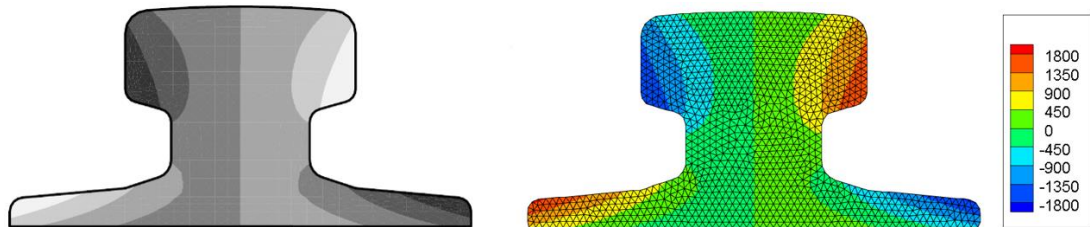


Figure 4.4: Comparison of the Warping Functions for the Rail Section (mm^2)

In this example, the obtained results show that cross-section properties, the shear flow diagram, shear stress values, and warping functions are consistent with those in the article [20] and the design specification document [28].

4.1.2. Elliptical Section

In Timoshenko and Goodier's book [11], an elliptical cross-section under a torsional moment is solved analytically. In this problem, solved herein, results for torsional shear stresses and warping functions are compared to the values in this book. The analytical formulations in Timoshenko and Goodier's book are given below. Respectively, a and b denote the long radius and short radius. M_t stands for applied torque in the problem. These parameters are shown in Figure 4.5.

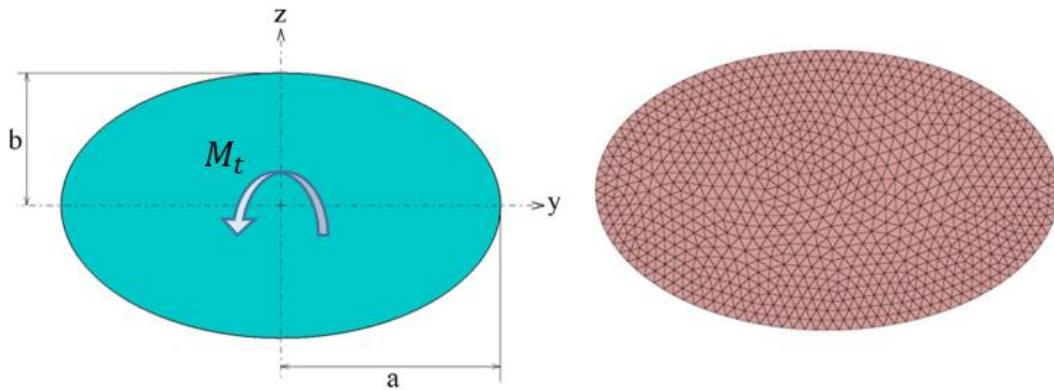


Figure 4.5: Geometrical Parameters and Meshed Model for the Elliptical Section

The torsional shear stresses and warping function in the book [11] are formulated as:

$$\tau_{xy} = -\frac{2M_t z}{\pi a b^3} \quad \tau_{xz} = \frac{2M_t y}{\pi a^3 b} \quad (4.1)$$

$$\omega = \frac{(b^2 - a^2)yz}{(b^2 + a^2)} \quad (4.2)$$

Following the analytical formulations, the finite element model is investigated. The cross-section is discretized by 2966 elements in Figure 4.5. To illustrate the inputs clearly, the geometrical data are given in Table 4.2. Based on these data, the shear stresses and warping function are solved by the formulations in Timoshenko's book and the FEM Study.

Table 4.2: Input Values for the Elliptical Section

Symbols	Inputs	Values
M_t	Torsional Moment (N.mm)	10000000
G	Shear Modulus (MPa)	28000
b	Short Radius (mm)	30
a	Long Radius (mm)	50

In Figure 4.6 and Table 4.3, the shear stress distribution and maximum shear stress values are illustrated, respectively.

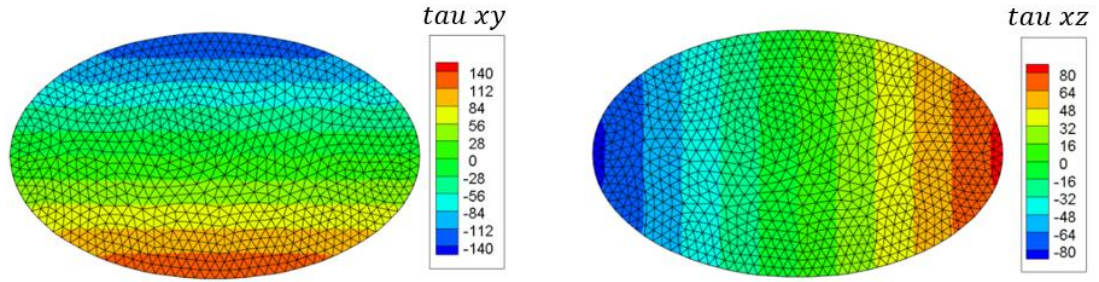


Figure 4.6: Shear Stress Distribution over the Elliptical Section (MPa)

Table 4.3: Comparison of the Shear Stresses over the Elliptical Section

Stress Component	Location (y,z)	The Book [11] (MPa)	Present Study (MPa)	Error (%)
τ_{xy}	(0, b)	-141.471	-139.941	1.08
τ_{xy}	(0, - b)	141.471	140.047	1.01
τ_{xz}	(a, 0)	-84.882	-84.304	0.68
τ_{xz}	(- a, 0)	84.882	84.243	0.75

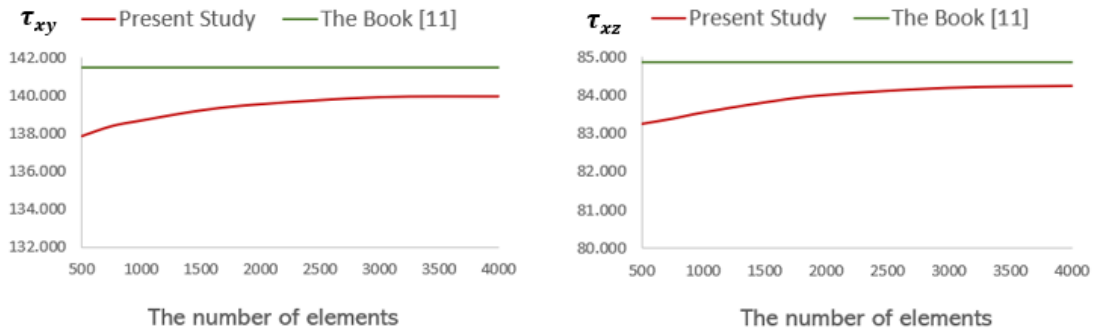


Figure 4.7: Variations of the Stresses in terms of the Number of Elements (MPa)

In this problem, a convergence test is performed to get the optimum stress results by increasing the number of mesh elements. In Figure 4.7, the variations of the shear stresses in the y and z directions are shown, respectively.

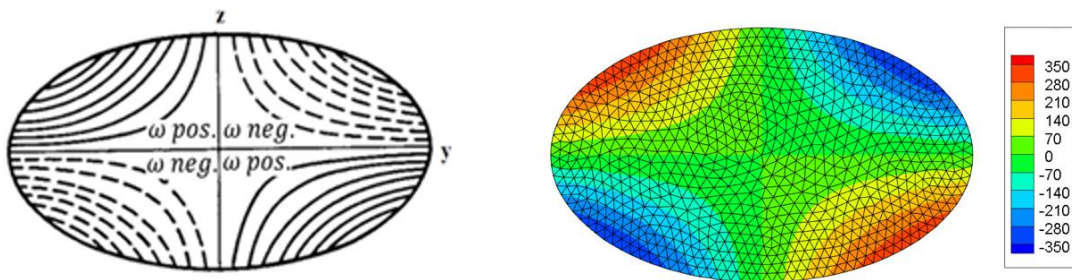


Figure 4.8: Comparison for the Warping Functions over the Elliptical Section (mm^2)

Table 4.4: Comparison of the Warping Functions over the Elliptical Section

	The Book [11] (mm^2)	Present Study (mm^2)	Error (%)
Maximum Warping Function Value	352.941	352.551	0.11
Minimum Warping Function Value	- 352.941	- 352.498	0.13

Lastly, Figure 4.8 shows that warping functions have the absolute maximum values at the corner regions. These values range between 352.941 mm^2 and -352.941 mm^2 . As shown in Table 4.4, the errors found for maximum and minimum warping values are 0.11% and 0.13%, respectively.

4.1.3. Variable Section

In this example, a beam having a variable cross-section is investigated under a distributed torsional moment. The dimensions of the cross-section are presented in Figure 4.9. This example was previously solved by Sapountzakis using the Boundary Element Method described in the author's article [26]. In this article, torsional and warping rigidities are obtained for the chosen sections. Moreover, the variations of normal and shear stresses along the beam due to Saint Venant torque, warping torque and warping moment are shown. The material properties are given in Table 4.5.

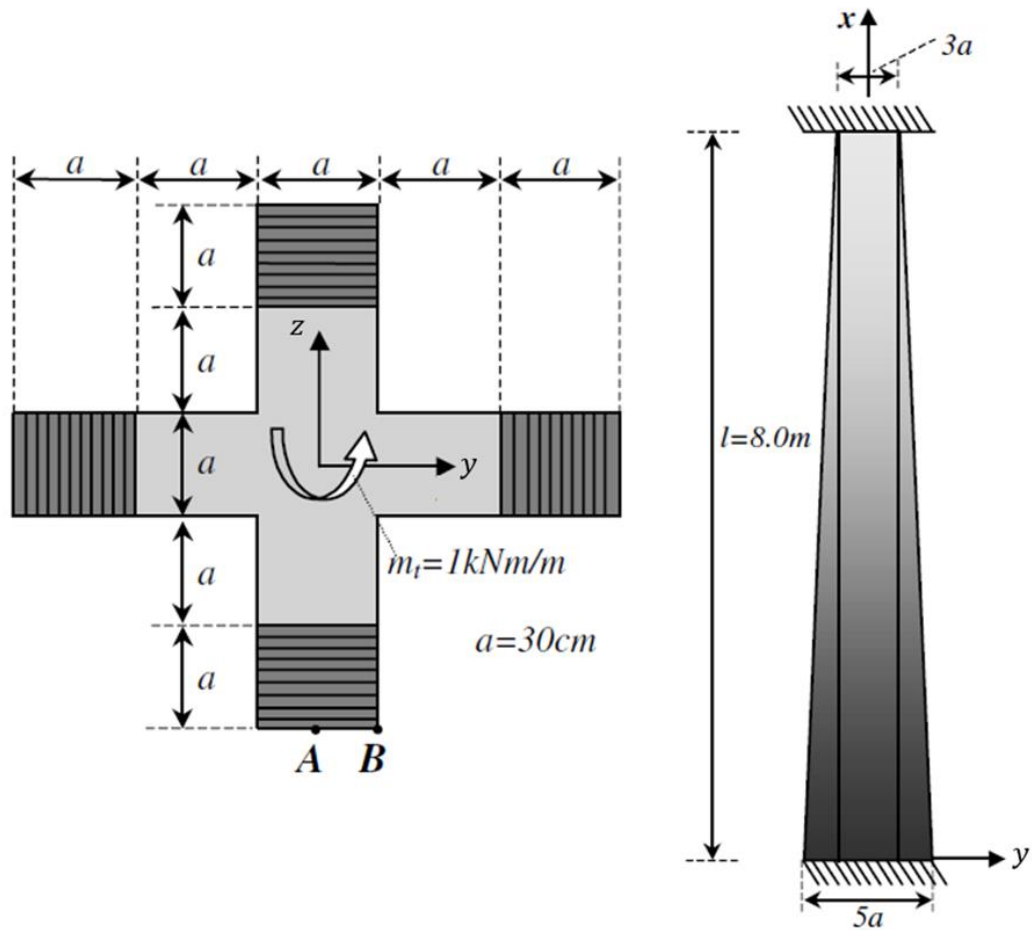


Figure 4.9: Geometrical Dimensions for the Beam of Variable Cross-section [26]

Table 4.5: Material Properties for the Beam of Variable Cross-section

Symbols	Name	Values
E	Elastic Modulus (MPa)	30000
G	Shear Modulus (MPa)	12500
ν	Possion Ratio	0.20

Firstly, the comparisons for torsional rigidity and warping rigidity are made with Sapountzakis's article [26]. In its formulized form, the torsional rigidity is defined as $G.J$; whereas, the warping rigidity is identified as $E.I_w$. While the torsional rigidities are checked in Table 4.6, the warping rigidities are matched in Table 4.7.

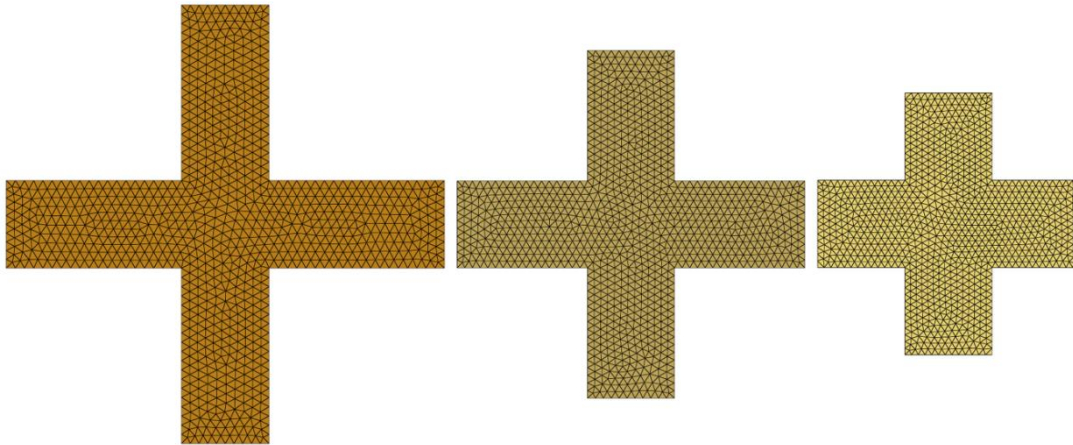


Figure 4.10: Cross-sections located at Fixed End 1 (left), Middle, Fixed End 2 (right)

In this example, the constraint at the larger cross-section is called fixed end 1 while the restriction at the smaller cross-section is referred to as fixed end 2. According to Table 4.6 and Table 4.7, there is a minor difference between BEM solution and FEM solution.

Table 4.6: Comparison of Torsional Rigidities for the Beam

Location	BEM Solution (N.mm ²)	FEM Solution (N.mm ²)	Difference (%)
Fixed End 1	3.29340E+14	3.33728E+14	1.33
Middle	2.60920E+14	2.64285E+14	1.29
Fixed End 2	1.89960E+14	1.92541E+14	1.36

Table 4.7: Comparison of Warping Rigidities for the Beam

Location	BEM Solution (N.mm ⁴)	FEM Solution (N.mm ⁴)	Difference (%)
Fixed End 1	3.05950E+19	3.04767E+19	0.39
Middle	1.35690E+19	1.34889E+19	0.59
Fixed End 2	3.98450E+18	3.93471E+18	1.25

Then, internal forces experienced along the beam must be determined. For this purpose, the beam is divided into 10 elements and 11 nodes, as in Figure 4.11. Each element has a length of 800 mm.

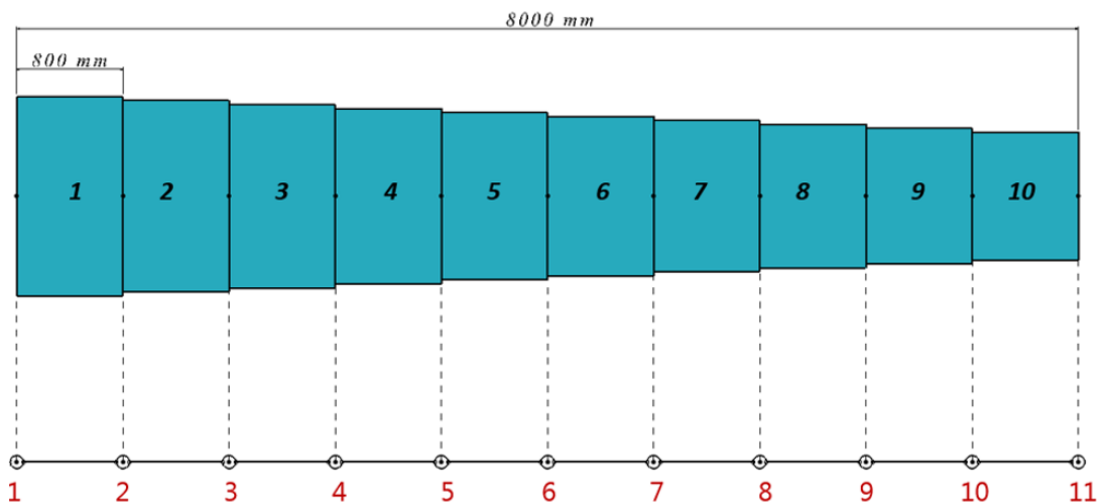


Figure 4.11: Discretization of the Beam

In Table 4.8, loads such as the SV torque, warping torque, and warping moment are tabulated for each node. It is clear that the maximum warping loads are appeared at the fixed ends. Disparately, the SV torque does not exist at these locations. Moreover, the warping loads have relatively smaller values at middle nodes than at fixed nodes.

Table 4.8: Internal Forces for the Beam

Node Number	St. Venant Torque (N)	Warping Torque (N)	Warping Moment (N)
1	0.0000E+00	3.8622E+06	-1.2351E+09
2	3.3104E+06	2.5269E+05	3.7362E+06
3	2.7205E+06	9.7921E+03	5.8948E+07
4	1.9313E+06	-4.5165E+03	5.8022E+07
5	1.1302E+06	-5.3237E+03	5.3892E+07
6	3.2838E+05	-5.3941E+03	4.9559E+07
7	-4.7379E+05	-5.4000E+03	4.5201E+07
8	-1.2763E+06	-5.4104E+03	4.0834E+07
9	-2.0790E+06	-5.6644E+03	3.6389E+07
10	-2.8534E+06	-2.8539E+04	2.7270E+07
11	0.0000E+00	-2.7426E+06	-4.8216E+08

After determining the internal forces, a cross-sectional analysis is carried out for each section. First, the change of the shear stress along the beam for point A is investigated. Then, the variation of the normal stress over the beam for point B is examined. Additionally, the stress graphs are obtained for the maximum stress cases.

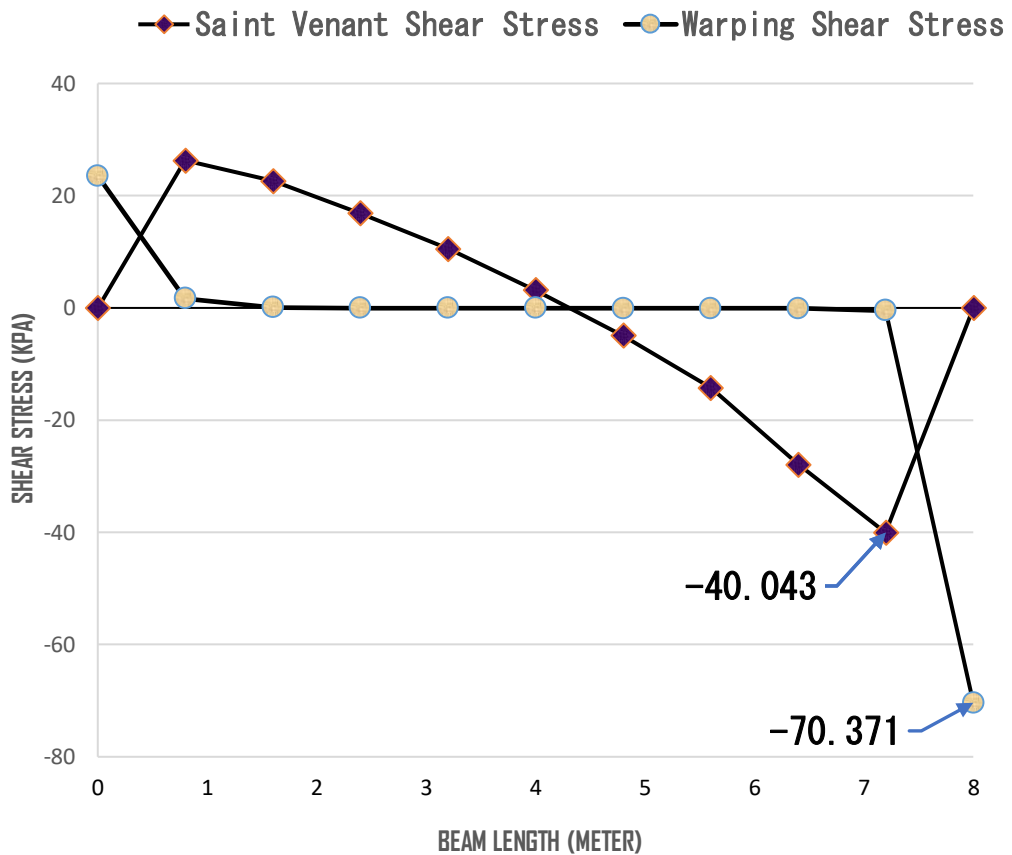


Figure 4.12: Variation of the Shear Stresses along the Beam at Point A

In Figure 4.12, the change of the shear stresses along the beam due to St. Venant torque and warping torque are illustrated for point A. The maximum stress arising from the warping torque is found as -70.371 kPa at fixed end 2. In Sapountzakis’s article this value is attained as -73.774 kPa. Moreover, the maximum value for the St. Venant torque is obtained as -40.043 kPa while the BEM solution results in -43.332 kPa. As such, the results found as a consequence of this thesis, as displayed in Figure 4.12, are significantly close to the results found by Sapountzakis. Besides, it is easily deduced from the graph in Figure 4.12 that the contribution of the shear stress due to warping torque should not be ignored.

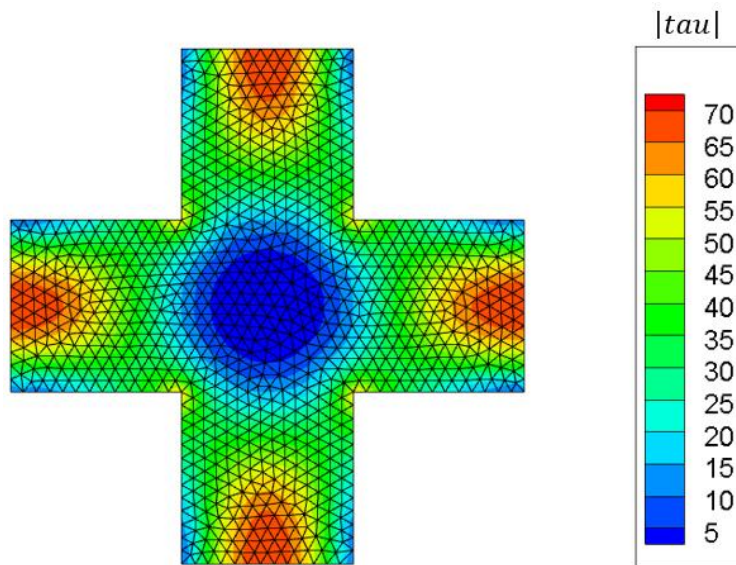


Figure 4.13: The Absolute Resultants of the Warping Shear Stresses (kPa)

In Figure 4.13, the absolute shear stress values for the warping torque are illustrated. At point A, the absolute value is observed as 73.774 kPa. Based on this figure, shear stress is not observed in the middle zone; this shear stress free zone is shaped like a circle.

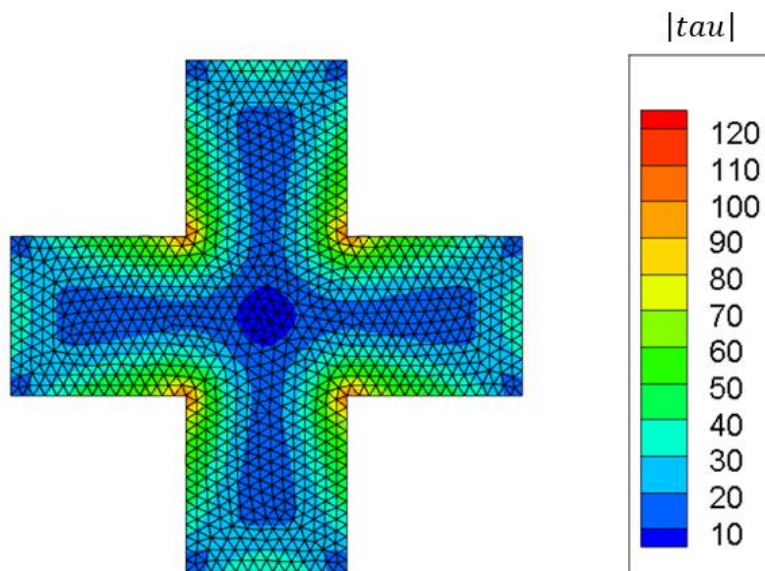


Figure 4.14: The Absolute Resultants of the St. Venant Shear Stresses (kPa)

In Figure 4.14, the absolute shear stress values for the St. Venant torque are displayed. At point A, the magnitude of the stress is stated as 43.332 kPa. Also, it is obvious that stress is concentrated at the innermost corners.

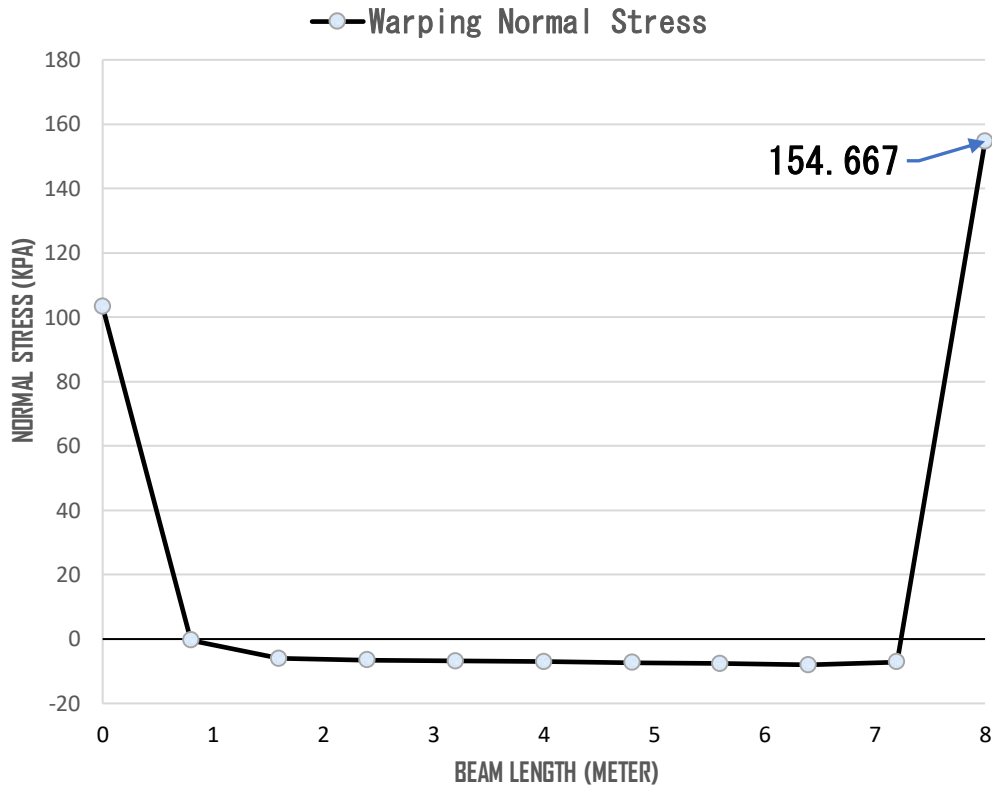


Figure 4.15: Variation of the Normal Stresses along the Beam at Point B

Lastly, the distribution of the normal stresses along the beam due to the warping moment is depicted in Figure 4.15 for point B. Based on this graph, the normal stress reaches the maximum value at fixed end 2, as it does for the warping shear stress. At this location, the normal stress is read as 154.667 kPa from the graph. In the BEM solution [26], it was found as 158.219 kPa. Furthermore, as it is seen in both Figure 4.12 and Figure 4.15, the effects of the warping decrease away from the fixed ends.

In Figure 4.16, the normal stress values due to warping moment are shown. At point B, the value is read as 154.667 kPa. Based on the figure, the maximum stress values occur at the outer corner regions.

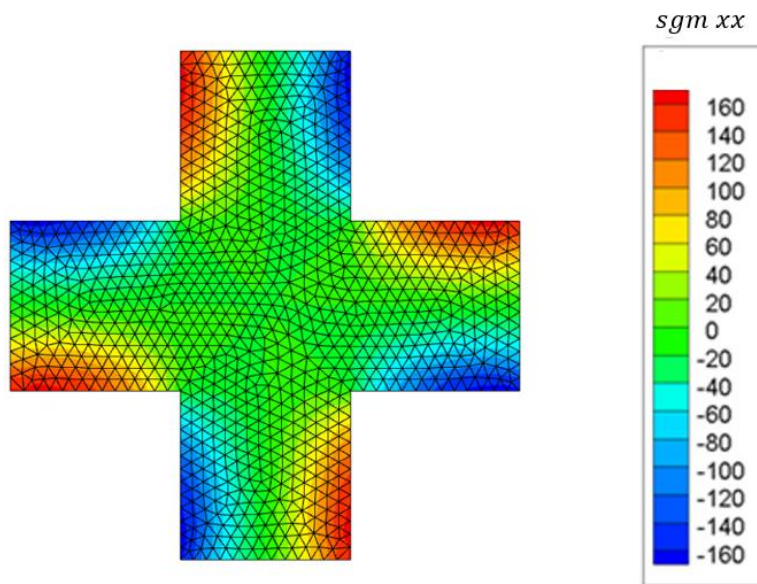


Figure 4.16: Distribution of the Normal Stresses (kPa)

4.2. Thick-walled Sections

4.2.1. Hollow Square Section

Structural elements with hollow square cross-sections are commonly used in several engineering systems such as automotive chassis, truss and framed structures, mechanisms, and robot arms. The torsional behavior of a square having hollow tubing sections is an important design consideration in many mechanical systems. If this section has thin walls, the analytical solutions for the torsional constant and torsional shear stress can be found in various design handbooks [25]. On the other hand, in the case of thick-walled cross-section, the problem must be solved by numerical methods, such as finite element analysis. In Figure 4.17, the change of torsional constant is shown in terms of the thickness/length ratio to decide whether the cross-section is thin-walled or thick-walled.

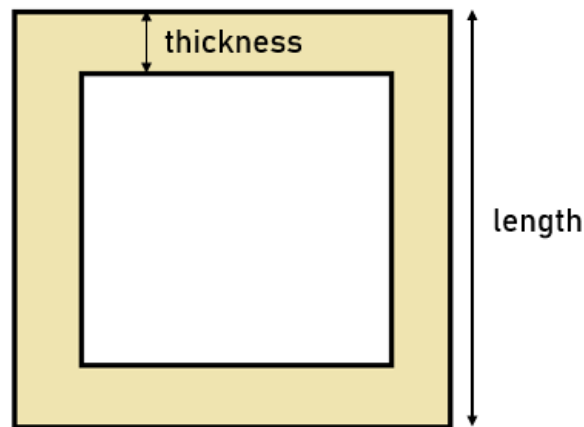


Figure 4.17: Hollow Square with Uniform Thickness

Thin walled Theory formulations by Roark [29] are;

$$J = t(a - t)^3 \quad (4.3)$$

$$\tau_{max} = T/2t(a - t)^2 \quad (4.4)$$

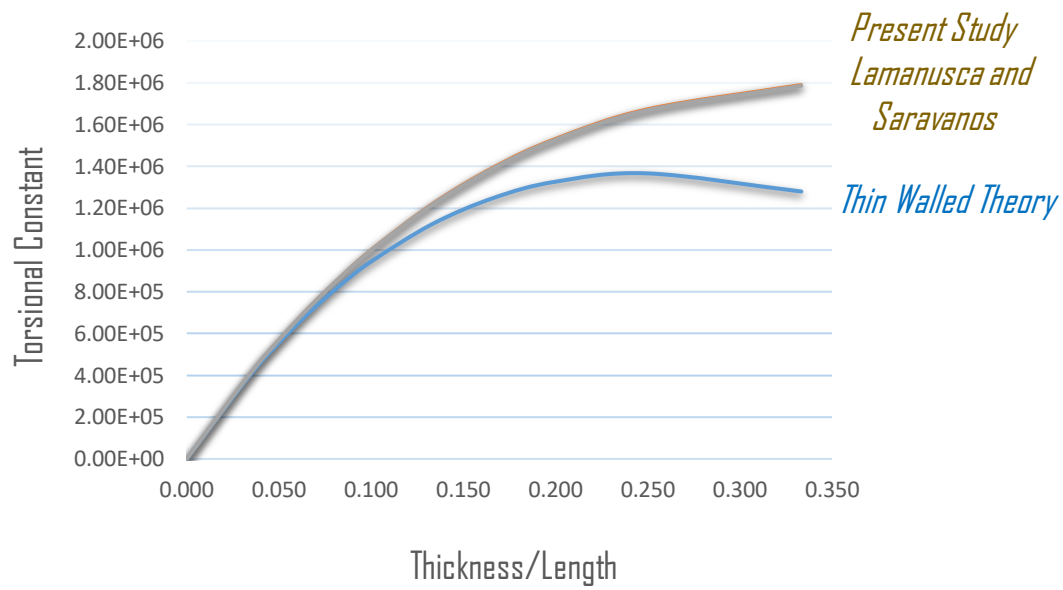


Figure 4.18: Distribution of the Torsional Constant in terms of Thickness/Length

As seen in Figure 4.18, when the thickness/length ratio is higher than 0.075, the values of torsional constants found by thin walled theory and within this study differ by 5%. In addition to this, when the thickness/length ratio is 0.240, the torsional constant starts to decrease. In other words, the thin-walled theory is strictly not applicable after this ratio. Lamanusca and Saravanos [25], and this study reach the same values at each point.

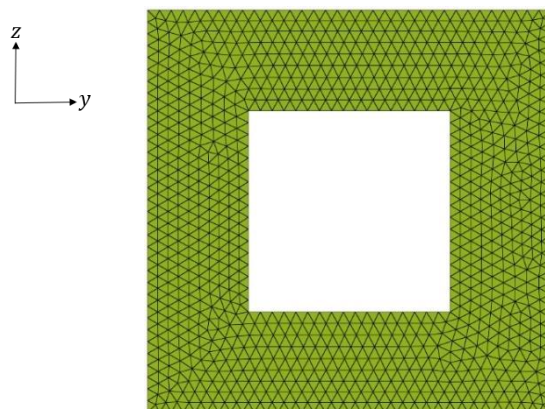


Figure 4.19: Discretization of the Hollow Square

Accordingly, in order to be able to evaluate a thick-walled problem the thickness/length ratio is selected as 0.250. Figure 4.19 depicts a hollow square with a 60 mm length and 15 mm thickness. The cross-section is discretized by 1211 elements. The applied load is 5×10^6 Nmm. The torsional constant and maximum shear stress values are compared with the article “The Torsional Analysis of Bars with Hollow Square Cross-Sections” by Lamanusca and Saravanos [25]. Said authors generated an algebraic formulation for torsional stiffness and maximum shear stress.

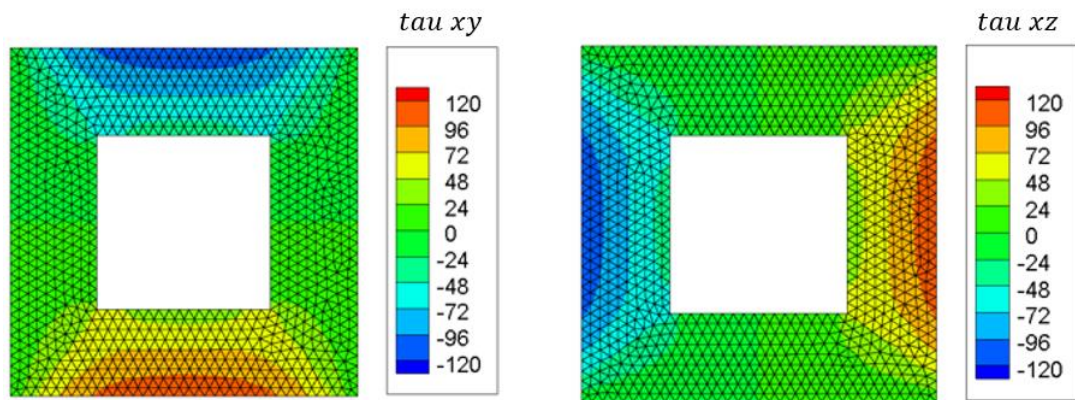


Figure 4.20: Shear Stress Distributions for the Hollow Square (MPa)

In Figure 4.20, according to the results, the maximum shear stresses are obtained as 112.3 MPa. This value is found as 110.1 MPa in the aforementioned article [25].

4.3. Thin-walled Open Sections

4.3.1. Channel Section

Channel beams are widely used in many engineering applications such as building structures and aircraft frames. The example problem analyzed herein is compared to the thesis entitled “Finite Element Stress Analysis of Elastic Beams under Non-Uniform Torsion” [21]. The example was validated analytically by a similar example in Chen and Atsuta [9]. The geometrical data for the example problem is given in Figure 4.21.

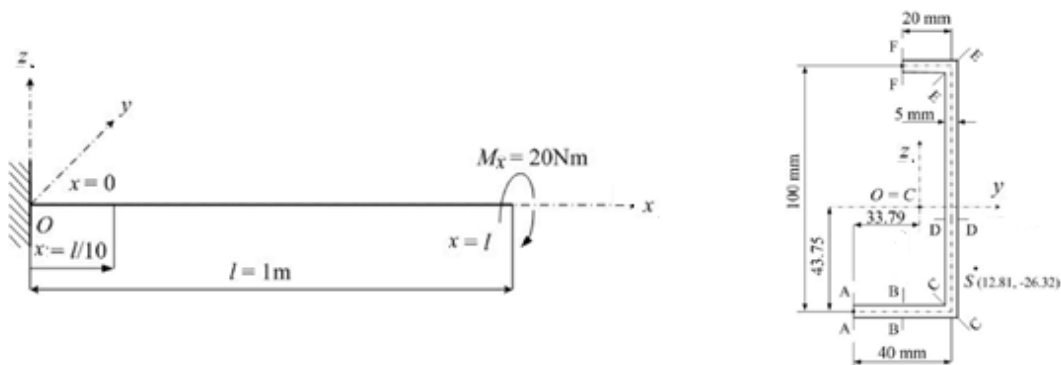


Figure 4.21: Channel Beam Problem under Torsional Moment [21]

Firstly, the internal forces along the beam are calculated. These forces are the St. Venant Torque, warping torque, and warping moment. Then, the normal and shear stress values are obtained for the A-B-C-D-E-F section cuts. The comparisons of stresses are at $x = 0$, $x = l/10$, and $x = l$.

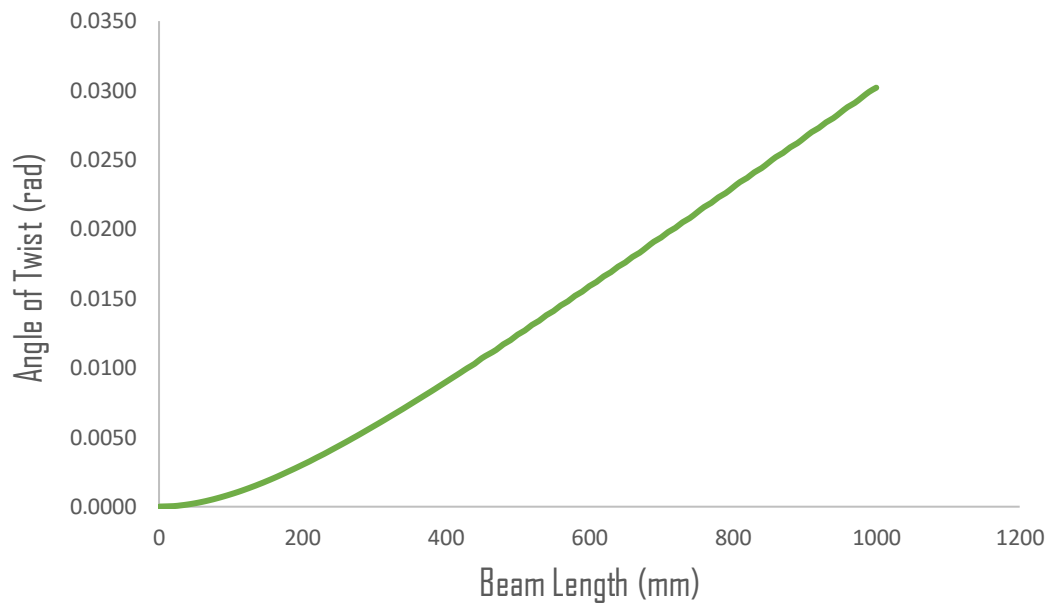


Figure 4.22: Distribution of the Angle of Twist

As can be seen from Figure 4.22, the angle of twist reaches a maximum value of 0.0302 rad. This value is the same as the aforementioned article [21].

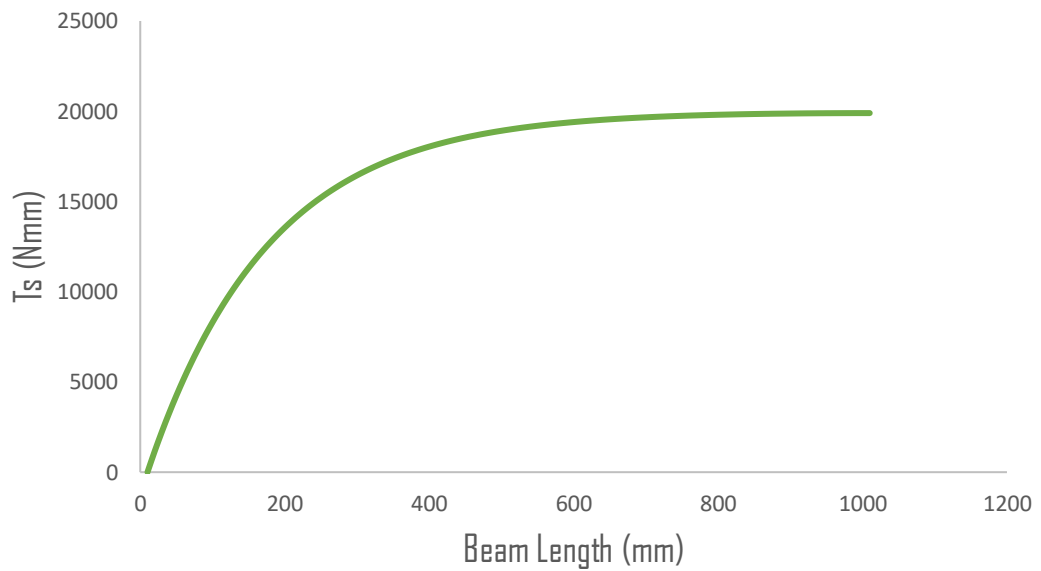


Figure 4.23: Distribution of the Saint Venant Torque

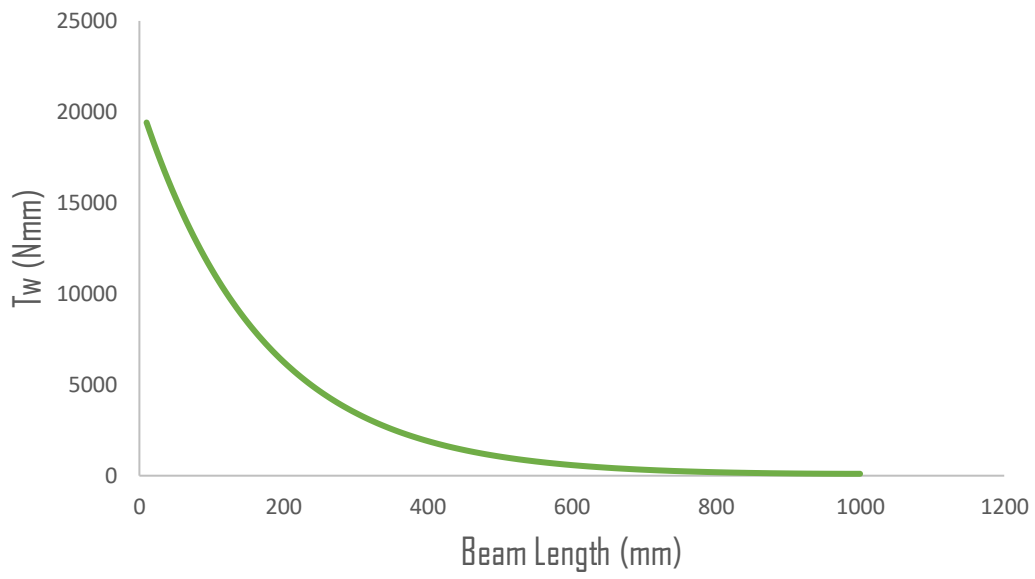


Figure 4.24: Distribution of the Warping Torque

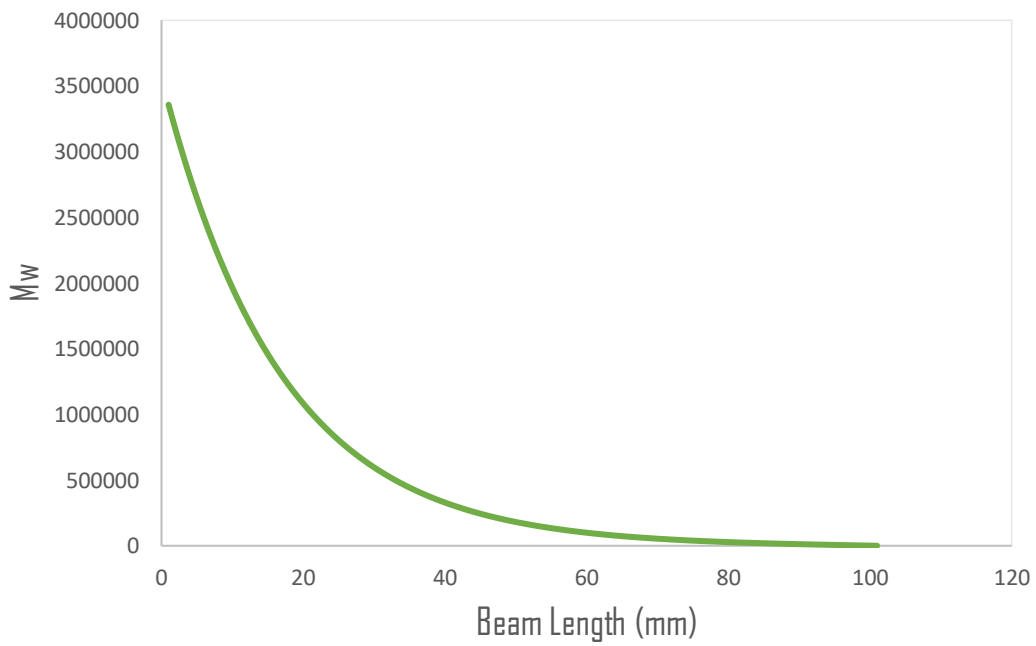


Figure 4.25: Distribution of the Warping Moment

As illustrated in Figure 4.23, Figure 4.24, and Figure 4.25, the maximum values of warping moment and warping torque are at the fixed end while the maximum value of Saint Venant Torque is obtained at the free end. Thus, the warping normal and shear stresses reach high values at the fixed point, but shear stresses due to Saint Venant torque have high values at the free end.

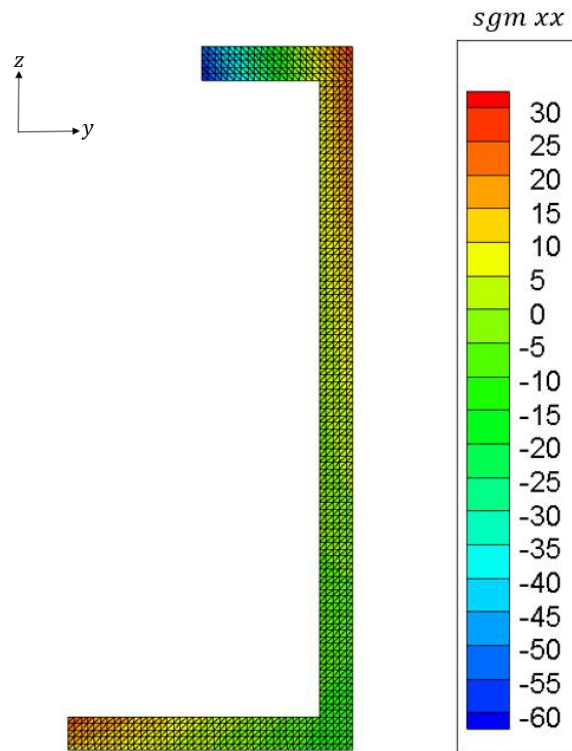


Figure 4.26: Stress Distribution for the Warping Moment at the fixed end (MPa)

Based on Figure 4.26, the magnitude of the normal stress peaks at the tip of the upper flange. The region at which the lower flange and the web intersects is stress-free. In Table 4.9, the stress values for section cuts A, C, E, and F are tabularized. These values are compatible.

Table 4.9: Comparison of the Warping Normal Stresses for the Channel Section

Section	Location	Numerical (MPa)	Analytical (MPa)
A-A	at x = 0 mm (fixed end)	18.39	18.07
C-C		-12.98	-12.82
E-E		18.69	18.87
F-F		-58.99	-59.58
A-A	at x = 100 mm	10.41	9.92
C-C		-7.41	-7.03
E-E		10.19	10.36
F-F		-33.34	-32.70
A-A	at x = 1000 mm (free end)	0.00	0.00
C-C		0.00	0.00
E-E		0.00	0.00
F-F		0.00	0.00

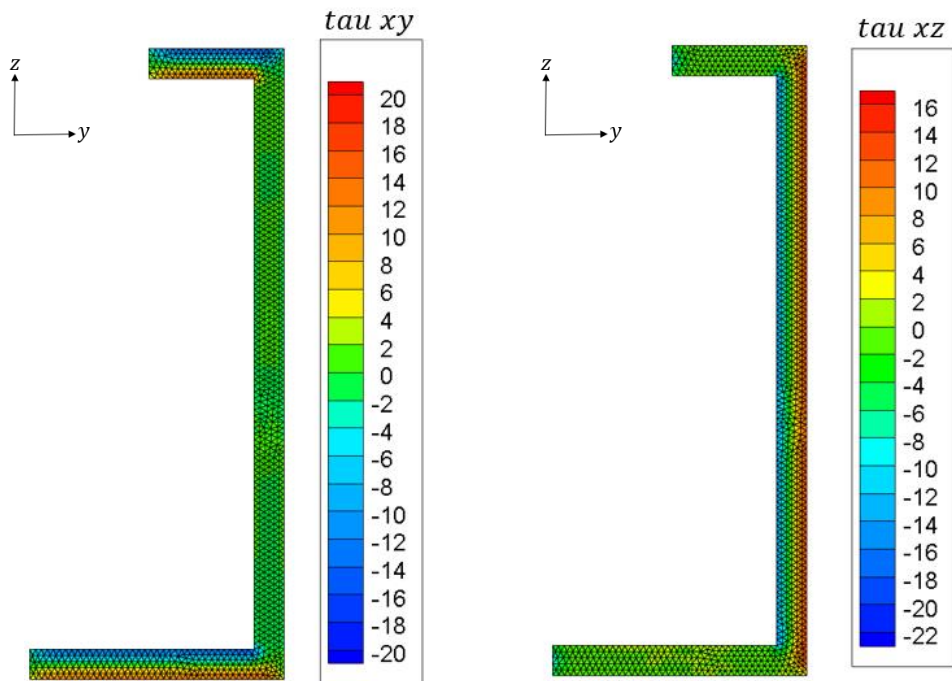


Figure 4.27: Stress Distribution for the St. Venant Torque at the free end (MPa)

Table 4.10: Comparison of the St. Venant Shear Stresses for Channel Section

Section	Location	Numerical (MPa)	Analytical (MPa)
B-B	at x = 0 mm (fixed end)	0.00	0.00
D-D		0.00	0.00
B-B	at x = 100 mm	6.27	6.79
D-D		6.27	6.79
B-B	at x = 1000 mm (free end)	13.91	14.97
D-D		13.91	14.97

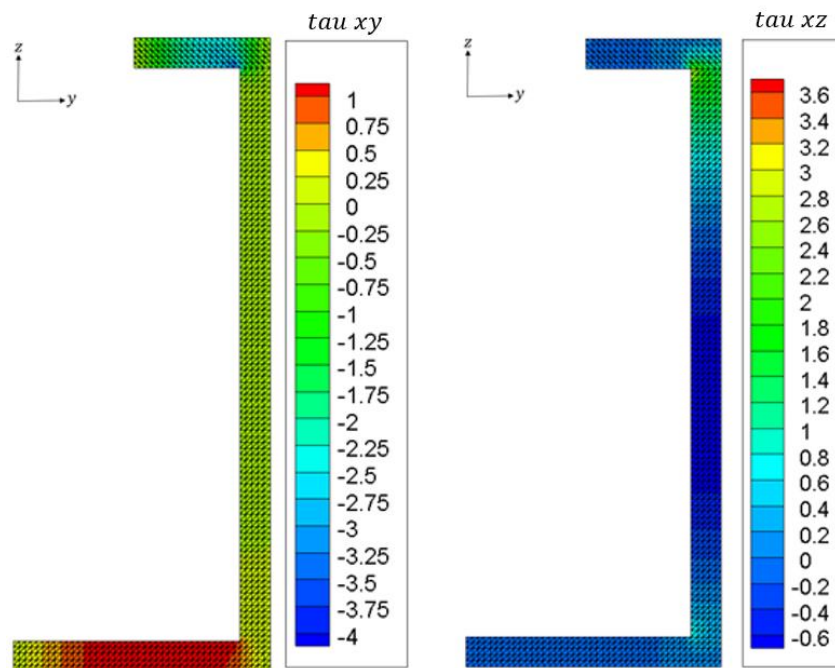


Figure 4.28: Stress Distribution for the Warping Torque at fixed end (MPa)

Table 4.11: Comparison of the Warping Shear Stresses for the Channel Section

Section	Location	Numerical (MPa)	Analytical (MPa)
B-B	at x = 0 mm (fixed end)	1.32	1.27
D-D		0.81	0.92
B-B	at x = 100 mm	0.65	0.70
D-D		0.59	0.51
B-B	at x = 1000 mm (free end)	0.00	0.00
D-D		0.00	0.00

The analysis results are consistent with the analytical solutions for St. Venant shear stresses, warping shear stresses, and warping normal stresses.

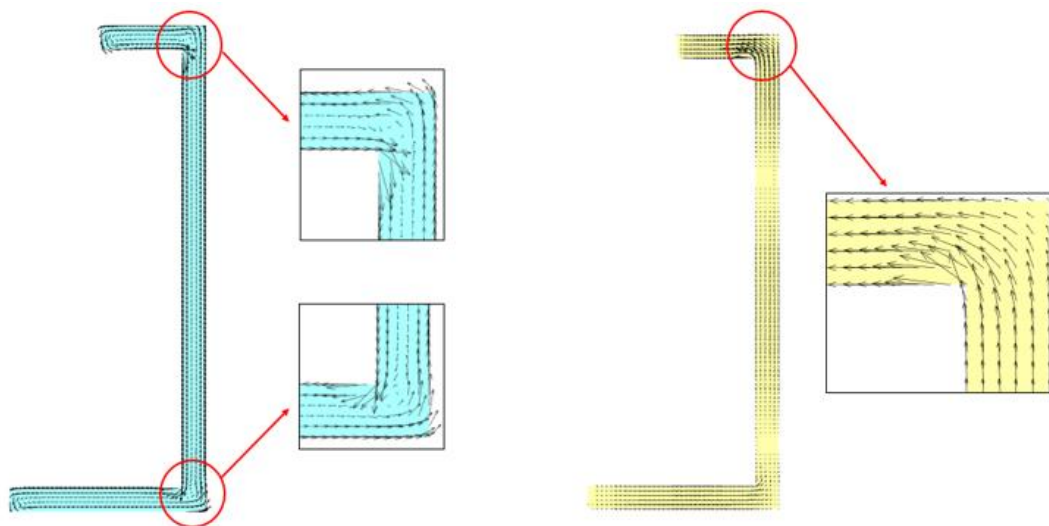


Figure 4.29: Shear Flows under St. Venant and Warping Torque

In Figure 4.29, the shear flows are indicated for shear stresses due to St. Venant and warping torques, respectively. In areas shown by red circles, stress concentration is observed. This undesired aspect is handled by filleting or chambering the radius.

4.4. Thin-walled Closed Sections

4.4.1. Multicell Section

Multicell sections are selected as thin-walled closed sections. This example is compared with a thin-walled analytical solution. The cross-section has outer dimensions of 60 mm x 100 mm, and a length of 300 mm. The wall thickness is 3 mm. In addition, both inner walls are centered according to the parallel walls. The material properties are given in Table 4.12.

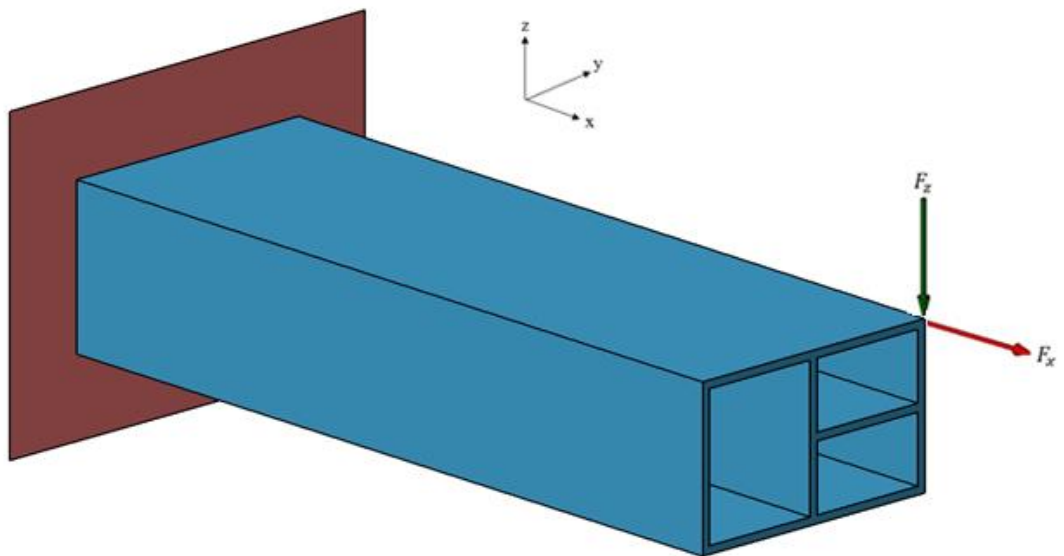


Figure 4.30: 3D Representation of the Multicell Section under Applied Loadings

Table 4.12: Material Properties for the Multicell Section

Symbols	Name	Values
E	Elastic Modulus (N.mm)	80000
G	Shear Modulus (MPa)	28000
ν	Possion Ratio	0.25

In Figure 4.31, the cross section is represented as thin-walled by its midlines. The cross-section is discretized by 2314 elements.

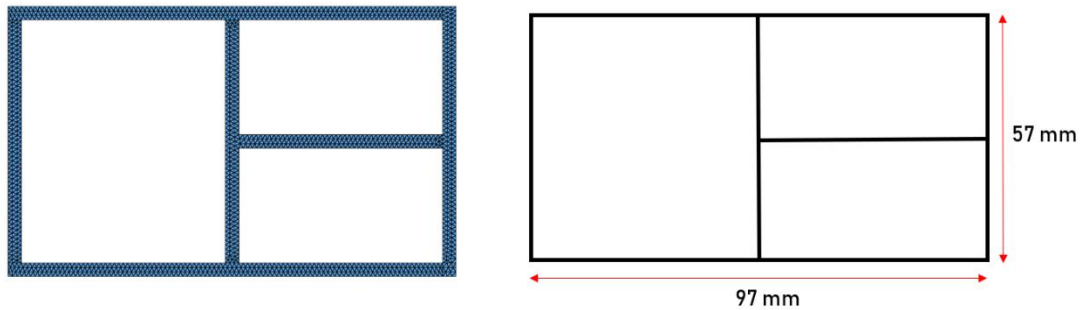


Figure 4.31: Thin-walled Representation of the Multicell Section

In Figure 4.32, the numbering used in the thin-walled solution is shown. In this figure, s denotes the distance from the starting point.

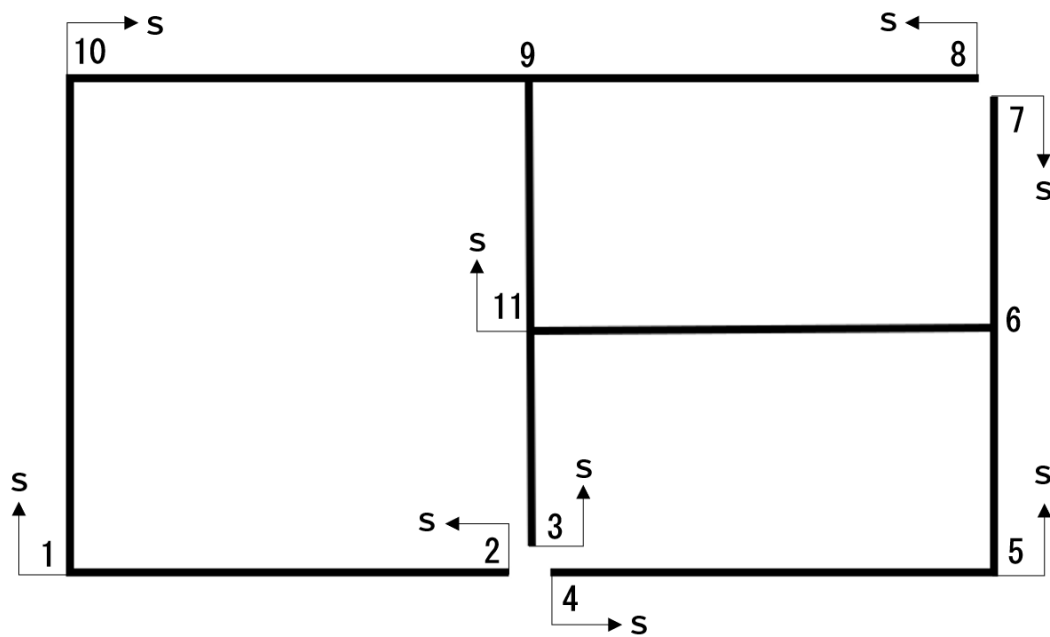


Figure 4.32: Numbering for the Thin-walled Solution

Table 4.13: Comparison of the Cross-section Properties for the Multicell Section

Property Name	Thin-walled Solution	Present Study	Difference (%)
Centroid, y_c (mm)	51.344	51.208	0.26
Centroid, z_c (mm)	28.500	28.500	0.00
Shear Center, y_s (mm)	-2.844	-2.569	6.15
Shear Center, z_s (mm)	0.000	0.000	0.00
Area (mm ²)	1.24100E+03	1.22250E+03	1.49
Inertia, I_{yy} (mm ⁴)	6.11624E+05	6.06000E+05	0.92
Inertia, I_{yz} (mm ⁴)	0.00000E+00	0.00000E+00	0.00
Inertia, I_{zz} (mm ⁴)	1.36485E+06	1.35735E+06	0.55
Torsional Constant (mm ⁴)	1.19103E+06	1.22202E+06	2.60
Warping Constant (mm ⁶)	4.02331E+07	4.30505E+07	7.00

In Table 4.13, a comparison of the thin-walled solutions and those found in the present study is made. In Table 4.14, internal forces are obtained for the free end. Based on these forces, a cross-sectional analysis is performed to determine the normal and shear stresses.

Table 4.14: Internal Forces for the Multicell Section

Internal Forces	Values (N)
N	10000
S_y	0
S_z	-3000
M_y	285000
M_z	-456560
T_s	-506832
T_w	345226
M_w	3647112

In Figure 4.33, the distribution of the warping functions and warped section are visualized. In Table 4.15, the maximum and minimum warping function are compared to the analytical solutions for Point 1 and 5.

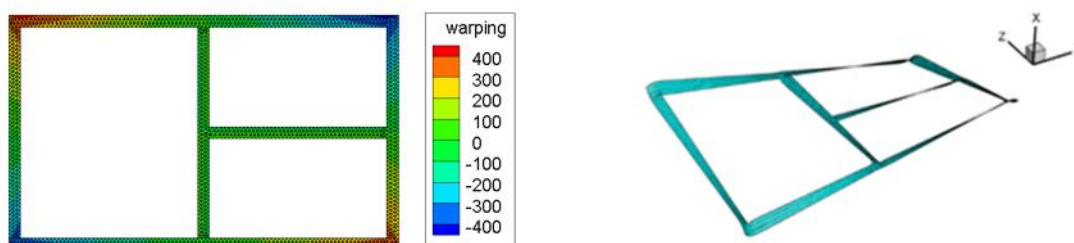


Figure 4.33: Distribution of the Warping Functions for the Multicell Section (MPa)

Table 4.15: Comparison of the Warping Functions for the Multicell Section

	Point	Thin-walled Solution (mm ²)	Present Study (mm ²)	Difference %
Minimum Warping Function	1	-359.026	-365.704	1.83
Maximum Warping Function	5	359.026	365.483	1.77

In Figure 4.34, the distribution of the shear stresses due to T_s and T_w are illustrated, respectively. In Table 4.16, the shear stress values for S_y , S_z , T_s , and T_w are matched with the analytical solutions for Point 2.

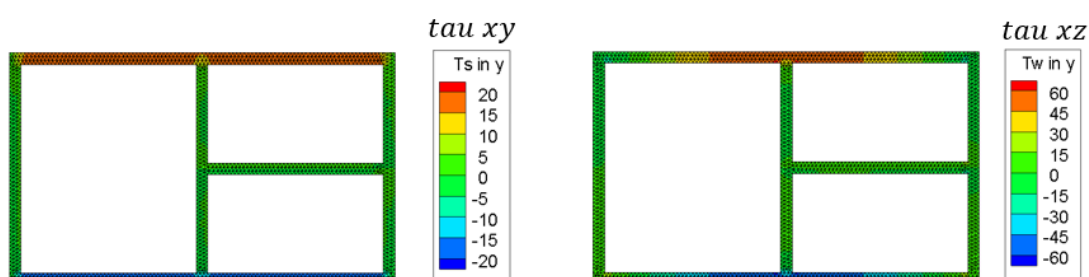


Figure 4.34: Distribution of the Shear Stresses of the Multicell Section (MPa)

Table 4.16: Comparison of the Shear Stresses of the Multicell Section

Forces	Point	Thin-walled Solution (MPa)	Present Study (MPa)	Difference %
S_y, S_z	2	-2.669	-2.517	5.70
T_s	2	-15.278	-15.312	0.22
T_w	2	-54.894	-53.993	1.64

In Figure 4.35, the distribution of the normal stresses due to N , M_y , M_z and M_w are shown, respectively. In Table 4.17, the normal stress values for N , M_y , M_z and M_w are checked with the analytical solutions for Point 8.

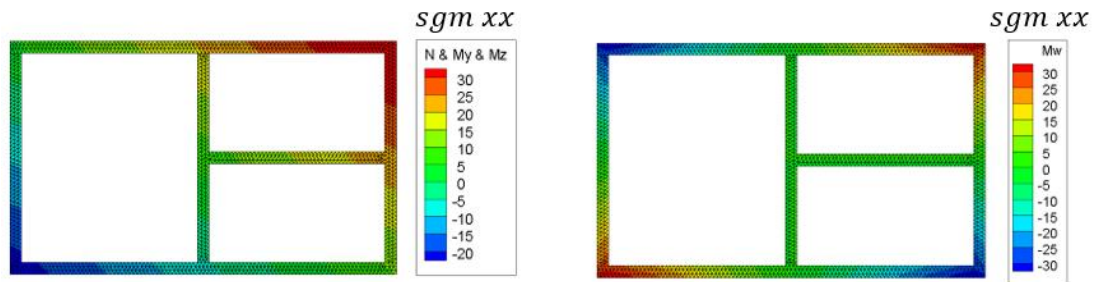


Figure 4.35: Distribution of the Normal Stresses of the Multicell Section (MPa)

Table 4.17: Comparison of the Normal Stresses of the Multicell Section

Forces	Point	Thin-walled Solution (MPa)	Present Study (MPa)	Difference %
N, M_y, M_z	8	36.611	36.505	0.29
M_w	8	32.981	31.695	3.90

In this example, the cross-section properties, warping functions, normal stresses, and shear stresses are compared with the thin-walled analytical solutions. All results are appropriately similar.

CHAPTER 5

CONCLUSIONS

5.1. Summary

The proposed finite element algorithm allows for conducting stress analyses of elastic beams with arbitrary cross-sections subjected to combined loadings. This study has consisted of five chapters, namely the Introduction, Literature Review, Formulations, Numerical Examples, and this chapter entitled, Conclusions. In Chapter 1, beams as a structural element are identified. The importance of cross-section properties and the uniform and non-uniform torsion theories are clarified. Moreover, the purpose and content of the thesis are expressed. In Chapter 2, related studies are offered in the form of a literature review by focusing on previous works. This chapter also includes the analytical and numerical approaches used to perform cross-sectional analyses. In Chapter 3, the formulations are given for the determination of internal forces and stresses. In the first part, equivalent loads are found at any cross-section along the beam. In the second part, 2D analysis is performed to obtain cross-section properties, warping functions, normal stresses, and shear stresses. In Chapter 4, beams with different cross-section types are analyzed to demonstrate the range of the applications of this study.

5.2. Conclusions

The results obtained in the examples affirm the developed finite element algorithm. All results are in a good agreement. In some problems, there are slight differences between analytical solutions and numerical solutions due to the number of elements and stress concentrations. These differences can be reduced by increasing the number of elements, and/or filleting or chamfering the sharp corners. The developed

formulations can aid mechanical engineers in regards to stress analysis of cross-sections while taking into consideration the warping effects.

5.3. Future Works

The effects of large axial forces on bending and torsion have not been covered in the present study. These effects can be included in future works.

REFERENCES

- [1] K. D. Polyzos (2018), “Detection and recognition of aerial targets via RADAR data processing, machine learning techniques and neural networks”.
- [2] M. Alexandrou (2015), “Difficulties in FE-modelling of an I beam subjected to torsion, shear and bending”.
- [3] B. Saint-Venant, “Memoire sur la torsion des prismes,” *Memoires des Savants Etrangers*, vol. 14, pp. 233–560, 1855.
- [4] V.Z. Vlasov, “Thin-Walled Elastic Bars” (in Russian), 2nd ed., Fizmatgiz, Moscow, 1959.
- [5] Carl T. Herakovich, “Mechanics IUTAM USNC/TAM: A History of People, Events, and Communities”, Springer International Publishing Switzerland 2016
- [6] E. Reissner and W. T. Tsai, ‘On the determination of the centers of twist and of shear for cylindrical shell beams’, *J. Appl. Mechanics* 39 1098–1102 (1972).
- [7] E. Trefftz, ‘“Uber den Schubmittelpunkt in einem durch eine Einzellast gebogenen Balken’, *ZAMM* 15, 220–225 (1935).
- [8] A. Weinstein, ‘The center of shear and the center of twist’, *Quart. of Appl. Math.* 5(1), 97–99 (1947).
- [9] W. F. Chen, T. Atsuta: *Theory of Beam-Columns, Volume 2: Space behavior and design*. J. Ross Publishing, Fort Lauderdale, FL 2008.

- [10] Hematiyan, M.R. and Doostfateme, A., “Torsion of Moderately Thick Hollow Tubes with Polygonal Shapes” , *Mechanics Research Communications*, 34, 528-537, 2007.
- [11] S. Timoshenko, J. Goodier: *Theory of Elasticity*. McGraw-Hill Co., NY, 1970.
- [12] J. J. Connor: *Analysis of Structural Member Systems*. Ronald Press, 1976.
- [13] Gjelsvik: *The Theory of Thin Walled Bars*. John Wiley & Sons, New York 1981.
- [14] M. A. Gurel, R. K. Pekgokgoz, M. Kısa, “An Approximate Torsion Analysis of Closed Moderately Thick-Walled, Thick-Walled, and Solid Cross-Sections.”, *Turkish J. Eng. Env. Sci.*32 (2008) , 277 – 287.
- [15] J. Francu, P. Novackova, P. Janicek, “Torsion of a Non-Circular Bar”. *Engineering Mechanics*, Vol. 19, 2012, No. 1, p. 45–60
- [16] Katori, H. (2016),” Determination of Shear Center of Arbitrary Cross-Section. “, *World Journal of Mechanics*.
- [17] Stronge, W.J. and Zhang, T.G. (1993) *Warping of Prismatic Bars in Torsion. International Journal of Solids and Structures*, **30**, 601-606.
- [18] B. D. Mixon (2008), “The Development of A Finite Element Tool For the Calculation of Beam Cross Section Properties.”
- [19] Gordon H. Holze, C. Paul Pulver and Yoseph Gebre-Giorgis, “Beam Cross Section Properties Determined by Boundary Element Analysis”, *SAE International*, Vol. 93, Section 3: 840403-840770 (1984), pp. 1019-1024
- [20] F. Gruttmann, W. Wagner and R. Sauer,” *Shear Stresses in Prismatic Beams with Arbitrary Cross-Sections*”, *Int. J. Num. Meth. Engng.*, 45 (1999), 865-889.
- [21] Banić D., Turkalj G., Brnić J. (2016),” *Finite Element Stress Analysis of Elastic Beams Under Non-Uniform Torsion*. “
- [22] V. Šimić: *Otpornost Materijala II. Školska knjiga*, Zagreb 1995.

- [23] A. Stefan, M. Lupoae, D. Constantin, C. Baci, "Numerical Determinations with Finite Differences Method of Prismatic Beams Subjected to Torsion", Proceedings of the World Congress on Engineering 2012 Vol III WCE 2012, July 4 - 6, 2012, London, U.K.
- [24] El Darwish, I. A. and Johnston, B. G., 1965, "Torsion of Structural Shapes," Journal of the Structural Division, Vol. 91, No. ST1 (Feb.), ASCE, New York, NY.
- [25] Lamancusa, J.S. and Saravanos, D.A., "The Torsional Analysis of Bars with Hollow Square Cross-Sections", Finite Elements in Analysis and Design, 6, 71-79, 1989.
- [26] E. J. Sapountzakis and V. G. Mokoš, "Nonuniform torsion of bars of variable cross section," *Computers and Structures* 82 (2004) 703–715.
- [27] W. D. Pilkey: Analysis and Design of Elastic Beams, Computational Methods. John Wiley & Sons, New York 2002.
- [28] DIN 536, A100 Crane Rail Design Specification, September 1991.
- [29] Warren C. Young and Richard G. Budynas, "Roark's Formulas for Stress and Strain", McGraw-Hill International Editions Series, 7th edition, 2002.

APPENDICES

A.1. DIN 536 Design Specification

UDC 621.87: 625.143.1-034.14-423 DEUTSCHE NORM September 1991

Crane rails Hot rolled flat bottom crane rails (type A) Dimensions, section parameters and steel grades	DIN 536 Part 1
--	------------------------------------

Kranschienen; Maße, statische Werte, Stahlsorten für Kranschienen mit Fußflansch Form A Supersedes December 1974 edition.

In keeping with current practice in standards published by the International Organization for Standardization (ISO), a comma has been used throughout as the decimal marker.

Dimensions in mm

1 Scope and field of application

This standard specifies requirements for hot rolled crane rails with a flat bottom (type A), with the dimensions specified in table 1 and made from steel with the properties specified in clause 4.

2 Dimensions and designation

2.1 Designation

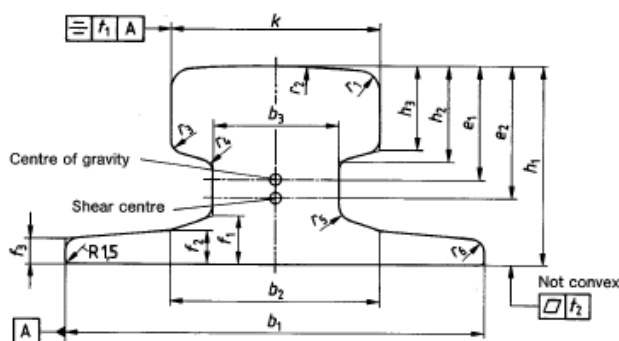


Figure 1: Type A crane rail

Designation of a flat bottom crane rail (type A) complying with this standard, with a head width, k , of 100 mm (A 100) and made from steel with a minimum tensile strength of 690 N/mm²:

Crane rail DIN 536 - A 100 - 690

Continued on pages 2 to 5.

ThyssenKrupp Stahl AG (EA-PL-KND):
 Vervielfältigung lt. DIN-Merkblatt 3 Ziffer 1
 © No part of this standard may be reproduced without the prior permission of DIN Deutsches Institut für Normung e.V., Berlin.
 In case of doubt, the German-language original should be consulted as the authoritative text.

2.2 Dimensions and tolerances

2.2.1 Crane rails shall be of the sizes and be subject to the limit deviations and geometrical tolerances specified in table 1. Any values for which no tolerance is specified shall be regarded as approximate values.

Table 1: Dimensions, limit deviations and geometrical tolerances (cf. subclause 2.2.1)

Crane rail symbol	k	b_1	b_2	b_3	f_1	f_2	f_3	h_1	h_2	h_3	r_1	$r_2^{3)}$	r_3	r_4	r_5	r_6	$t_1^1)$	$t_2^2)$			
	Limit-deviations	Limit-deviations						Limit-deviations													
A 45	45	$\pm 0,6$	125	$\begin{smallmatrix} +1,5 \\ -3 \end{smallmatrix}$	54	24	14,5	11	8	55	± 1	24	20	4	400	3	4	5	4	2	$\begin{smallmatrix} +0,6 \\ 0 \end{smallmatrix}$
A 55	55	$\pm 0,6$	150	$\begin{smallmatrix} +1,5 \\ -3 \end{smallmatrix}$	66	31	17,5	12,5	9	65	± 1	28,5	25	5	400	5	5	6	5	2	$\begin{smallmatrix} +0,6 \\ 0 \end{smallmatrix}$
A 65	65	$\pm 0,8$	175	$\begin{smallmatrix} +1,5 \\ -4 \end{smallmatrix}$	78	38	20	14	10	75	± 1	34	30	6	400	5	5	6	5	2	$\begin{smallmatrix} +0,6 \\ 0 \end{smallmatrix}$
A 75	75	$\pm 0,8$	200	$\begin{smallmatrix} +2 \\ -5 \end{smallmatrix}$	90	45	22	15,4	11	85	± 1	39,5	35	8	500	6	6	8	6	2	$\begin{smallmatrix} +0,8 \\ 0 \end{smallmatrix}$
A 100	100	± 1	200	$\begin{smallmatrix} +2 \\ -5 \end{smallmatrix}$	100	60	23	16,5	12	95	$\pm 1,5$	45,5	40	10	500	6	6	8	6	3	$\begin{smallmatrix} +0,8 \\ 0 \end{smallmatrix}$
A 120	120	± 1	220	$\begin{smallmatrix} +2 \\ -5 \end{smallmatrix}$	120	72	30	20	14	105	$\pm 1,5$	55,5	47,5	10	600	6	10	10	6	3	$\begin{smallmatrix} +1,0 \\ 0 \end{smallmatrix}$
A 150	150	± 1	220	$\begin{smallmatrix} +2 \\ -5 \end{smallmatrix}$	-	80	31,5	-	14	150	$\pm 1,5$	64,5	50	10	800	10	30	30	6	3	$\begin{smallmatrix} +1,0 \\ 0 \end{smallmatrix}$

1) Cf. subclauses 2.2.2 and 2.2.4. 2) Cf. subclauses 2.2.3 and 2.2.4. 3) Cf. Explanatory notes

3.2 The mass of crane rails, as a function of the section parameters, shall be as specified in table 2.

Table 2: Mass and section parameters

Crane rail symbol	Mass, in kg/m	Section parameters ¹⁾									
		e_1 cm	e_2 cm	A_x cm ²	A_y cm ²	A_z cm ²	I_x cm ⁴	I_y cm ⁴	I_z cm ⁴	\bar{S}_y cm ³	\bar{S}_z cm ³
A 45	22,1	3,33	4,24	28,2	17,0	9,6	39	90	170	22,88	26,12
A 55	31,8	3,90	4,91	40,5	24,8	14,6	88	178	337	38,45	48,64
A 65	43,1	4,47	5,61	54,9	33,7	20,2	173	319	606	60,18	69,22
A 75	56,2	5,04	6,29	71,6	44,1	26,9	311	531	1011	88,41	102,09
A 100	74,3	5,29	6,27	94,7	65,8	41,6	666	856	1345	128,78	141,58
A 120	100,0	5,79	6,53	127,4	97,1	58,5	1302	1361	2350	187,23	222,35
A 150	150,3	7,73	8,48	191,4	153,6	107,1	2928	4373	3605	412,00	342,60

1) In accordance with DIN 1080 Parts 1 and 2, the symbols have the following meaning.

A_x cross-sectional area

A_y, A_z surfaces subjected to shear

I_x second moment of area (torsion)

I_y, I_z second moments of area (flexure)

\bar{S}_y, \bar{S}_z static moments of parts of cross sections delineated by and related to the principal axes